

# Basin-scale fluvial correlation and response to the Tethyan marine transgression: An example from the Triassic of central Spain

Maximilian Franzel<sup>1</sup>  | Stuart J. Jones<sup>1</sup> | Neil Meadows<sup>2</sup> | Mark B. Allen<sup>1</sup> | Ken McCaffrey<sup>1</sup> | Tim Morgan<sup>3</sup>

<sup>1</sup>Department of Earth Sciences, Durham University, Durham, UK

<sup>2</sup>Redrock International Limited, Wirral, UK

<sup>3</sup>Chemostrat Ltd, Welshpool, UK

## Correspondence

Maximilian Franzel, Department of Earth Sciences, Durham University, Durham, UK.  
Email: maximilian.franzel@durham.ac.uk

## Funding information

Natural Environment Research Council, Grant/Award Number: NE/M00578X/1

## Abstract

The relationships between large-scale depositional processes and the stratigraphic record of alluvial systems, e.g. the origin and distribution of channel stacking patterns, changing architecture and correlation of strata, are still relatively poorly understood, in contrast to marine systems. We present a study of the Castillian Branch of the Permo-Triassic Central Iberian Basin, north-eastern Spain, using chemostratigraphy and a detailed sedimentological analysis to correlate the synrift Triassic fluvial sandstones for ~80 km along the south-eastern basin margin. This study investigates the effects of Middle Triassic (Ladinian) Tethyan marine transgression on fluvial facies and architecture. Chemostratigraphy identifies a major, single axially flowing fluvial system lasting from the Early to Middle Triassic (~10 Ma). The fluvial architecture comprises basal conglomerates, followed by amalgamated sandstones and topped by floodplain-isolated single- or multi-storey amalgamated sandstone complexes with a total thickness up to ~1 km. The Tethyan marine transgression advanced into the basin with a rate of 0.04–0.02 m/year, and is recorded by a transition from the fluvial succession to a series of maximum flooding surfaces characterised by marginal marine clastic sediments and sabkha evaporites. The continued, transgression led to widespread thick carbonate deposition infilling the basin and recording the final stage of synrift to early-post-rift deposition. We identify the nonmarine to marine transition characterised by significant changes in the Buntsandstein succession with a transition from a predominantly tectonic- to a climatically driven fluvial system. The results have important implications for the temporal and spatial prediction of fluvial architecture and their transition during a marine transgression.

## KEYWORDS

Buntsandstein, Central Iberian Basin, Chemostratigraphy, fluvial, marine transgression, Triassic

This is an open access article under the terms of the Creative Commons Attribution License, which permits use, distribution and reproduction in any medium, provided the original work is properly cited.

© 2020 The Authors. *Basin Research* published by International Association of Sedimentologists and European Association of Geoscientists and Engineers and John Wiley & Sons Ltd

# 1 | INTRODUCTION

This study describes the fluvial stratigraphic responses to marine transgression in the Central Iberian Basin (CIB), Spain, before and during the Middle Triassic (Ladinian), with the aim of understanding how and why fluvial architecture changed over time.

Stratal geometries and the distribution of depositional systems in paralic settings record differences in sedimentary processes and basin development as sea level changes (e.g. Burns, Heller, Marzo, & Paola, 1997; Posamentier, Jervey, & Vail, 1988; Posamentier & Vail, 1988). Relationships between large-scale depositional processes and the stratigraphic record are relatively well understood for marine deposits, but less so for fluvial systems. For example, the origin and distribution of channel stacking patterns in alluvial–fluvial strata and their direct relationship to sea level changes is controversial (Hartley & Evenstar, 2018; Heller & Paola, 1996; Pisel, Pyles, & Kirschbaum, 2018; Shanley & McCabe, 1991, 1994).

Fluvial sediments aggrade during relative rises and/or highstands in sea level. The maximum extent and geometry of the coastal onlap during a marine transgression is controlled by the amount and rate of accommodation space creation upstream of the shoreline and direct competition with sediment supply of the fluvial system. It is important to understand how deposition of the fluvial sediments responds to changes in relative sea level, to inform models of fluvial and coastal plain facies distribution and connectivity used for hydrocarbon exploration, carbon capture and storage and aquifer studies.

An issue in understanding the effects of relative sea level rise on fluvial stratigraphy is the difficulty in correlating and dating fluvial successions. Chemostratigraphy or ‘chemical stratigraphy’ has been used for several decades in the oil and gas industry to support stratigraphic correlation of wells across areas of poor subsurface information availability. It has also worked for outcrop studies, particularly in fluvial systems (e.g. Ellwood, Tomkin, Ratcliffe, Wright, & Kafafy, 2008; Hildred, Ratcliffe, Wright, Zaitlin, & Wray, 2010; Newell, 2018; Pearce, Besly, Wray, & Wright, 1999; Ratcliffe et al., 2015; Ratcliffe et al., 2010; Svendsen, Friis, Stollhofen, & Hartley, 2007; Wright, Ratcliffe, Zaitlin, & Wray, 2010). The approach involves the geochemical characterisation and correlation of strata by using major and trace element geochemistry and is very useful when applied to sequences with poor biostratigraphic control, in particular for fluvial ‘red bed’ sequences. The tool can be used to model changes in sediment provenance, palaeoclimate and sediment supply input (Davies et al., 2013; Pearce, Martin, Cooper, & Wray, 2010; Ratcliffe et al., 2015).

The results presented in this study are based on a detailed sedimentological field study in combination with a

## Highlights

- Detailed sedimentology and chemostratigraphy allowed a high-resolution spatial and temporal correlation of Triassic synrift fluvial sandstones.
- A single major fluvial system along the rifted basin margin that was long-lived for ~10 Ma has been identified using detailed chemostratigraphy.
- We argue that the Tethyan marine transgression is accompanied by a transition from a predominantly tectonic- to a climatically-driven fluvial system.
- The onset of the Tethyan marine transgression caused rapid shut down of clastic fluvial input into the basin with a series of maximum flooding surfaces characterised by marginal marine sediments.

high-resolution chemostratigraphic analysis of the Triassic fluvial sediments (Buntsandstein) in the Castillian branch of the Iberian Ranges, north-eastern Spain. Excellent exposures enable a high-resolution study with the aims of (a) correlating synrift Triassic fluvial sandstones for ~80 km along the SE margin of the CIB; (b) exploring changes and trends in the sediment composition to infer variations in sediment provenance, palaeoclimate and/or weathering; (c) investigating the effects of Middle Triassic (Ladinian) marine transgression on fluvial facies and architecture and implications for understanding sedimentation in rift basins during a terrestrial–marine transition.

## 2 | GEOLOGICAL SETTING AND BASIN STRATIGRAPHY

In early Permian times, the Iberian Peninsula occupied the central-eastern side of Pangea, in the southernmost part of the Laurasia megacontinent and near the western margin of the Tethys Sea (Borrueal-Abadía et al., 2015; De la Horra et al., 2012). The breakup of Pangea led to the development of three main rift systems (Catalonia-Valencia-Prebetic, Pyrenean-Asturian and Iberian Basins) in Iberia, which continued to the middle Cretaceous, until the Peninsula was separated from the European continent (Salas et al., 2001). Compressional tectonics related to the Pyrenean orogeny in the Late Cretaceous-Palaeogene accreted the Iberian Plate back to the Eurasian continent and inverted most of its Mesozoic rift systems (Salas et al., 2001).

The Iberian Basin developed as a fault-bound, intracratonic rift basin during the early-middle Permian and is bound to the north by the Ebro Basin, to the west by the Tajo Basin and in the south by the La Mancha Basin (De Vicente et al., 2009). Its geological history is shaped by three rifting

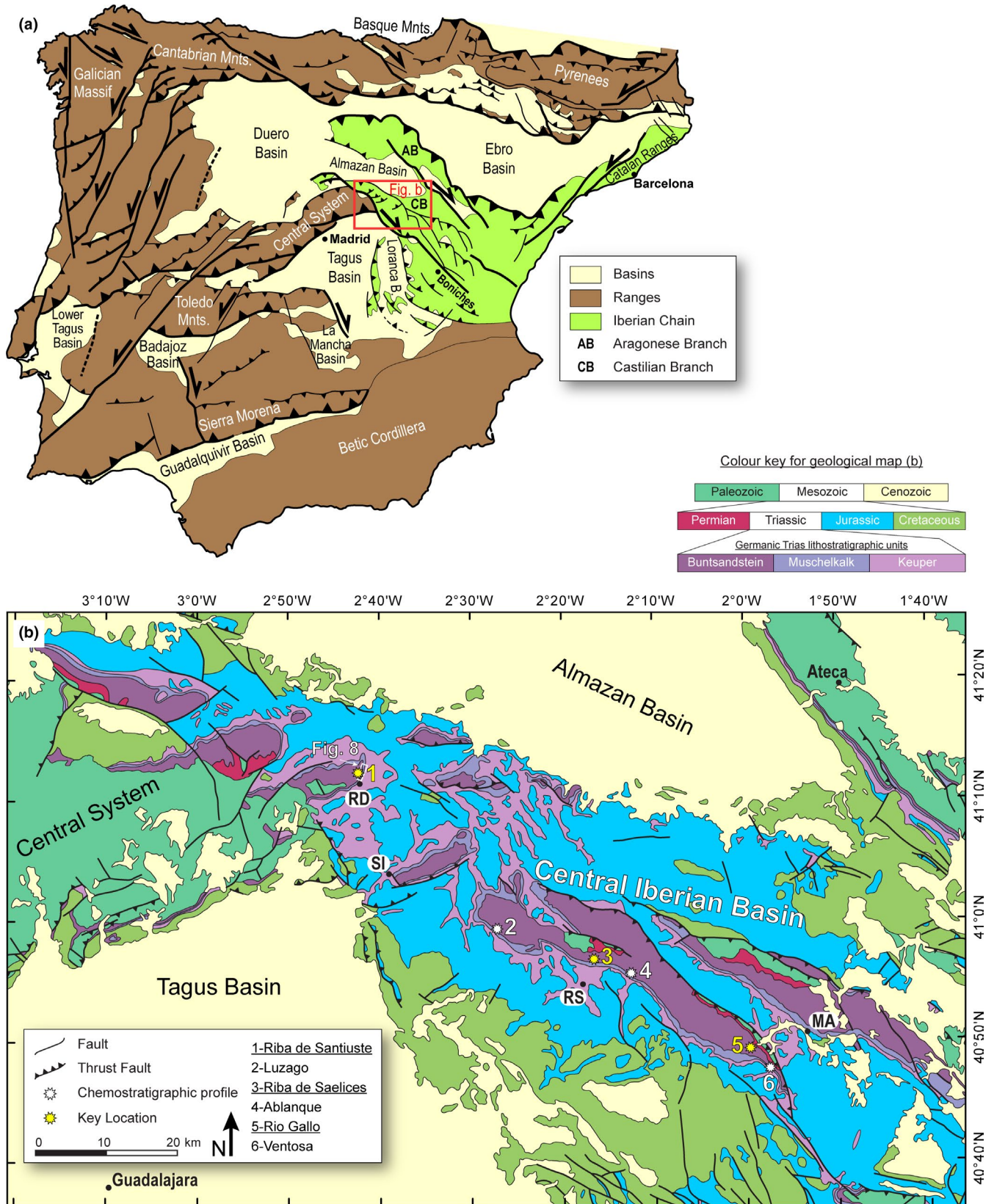


**FIGURE 1** (a) Generalised map showing the tectonic configuration of the Iberian Peninsula and its basins and ranges (map after De Vicente et al., 2009). (b) Schematic geological map of the Castilian Branch of the Iberian Ranges showing the areas of fieldwork and the chemostratigraphic sections (map modified after Fernández et al., 2015). Abbreviations used for towns and villages are MA, Molina de Aragon; RD, Riba de Santiuste; RS, Riba de Saelices; SI, Sigüenza

phases from the early Permian to the Middle Triassic with increasing thermal subsidence rates towards the end of rifting (López-Gómez, Arche, Vargas, & Marzo, 2010). Two compressional tectonic events in the Palaeogene are related to the collision of the Iberian craton with Europe and the Pyrenean and early Betic orogeny; these events uplifted the present Iberian Ranges (Arche & López-Gómez, 1996; López-Gómez & Arche, 1993a, 1993b; Salas et al., 2001). A linear fold and thrust belt along the north-eastern edge of the Iberian microplate developed, separated into two NW-SE striking arches (Aragonian Branch and Castillian Branch) separated by the Almazan Basin (Figure 1) (Arche & López-Gómez, 2005; Salas et al., 2001). The development of these belts was controlled by the activity of the basin boundary faults, which were normal faults during Mesozoic times and reverse faults during the Oligocene-Miocene compressional stages (López-Gómez et al., 2012; Salas & Casas, 1993). This extensive tectonic overprint resulted in folding and thrusting of the Mesozoic strata. Quaternary erosion has created a morphology dominated by fluvial incision and canyons (De Vicente et al., 2009).

The sections in this study are situated near the north-western margin of the Iberian Ranges in the Castillian Branch, at the southern margin of the CIB. The Triassic sediments in the study area are equivalent to the Germanic Trias lithostratigraphic units of Buntsandstein and Muschelkalk and were deposited into half grabens during the rifting phases (García-Lasanta et al., 2015).

Late Permian Saxonian sediments in the south-eastern Iberian Ranges (Boniches) and Buntsandstein Facies in the northwest (Riba de Santiuste and Molina de Aragon) unconformably overly metamorphic basement. This basement consists of Cambrian-Silurian slates and quartzites, deformed by the Hercynian orogeny (Arche & López-Gómez, 1999a, 1999b; López-Gómez, Arche, & Pérez-López, 2002). The Early to Middle Triassic Buntsandstein sediments are characterised by continental red beds with a conglomeratic base that changes to finer-grained sandy facies upward (Ramos, Sopena, & Perez-Arlucea, 1986). The Tethyan transgression in the Middle Triassic (Figure 2) overlies the basin-wide Buntsandstein and forms marine carbonates of

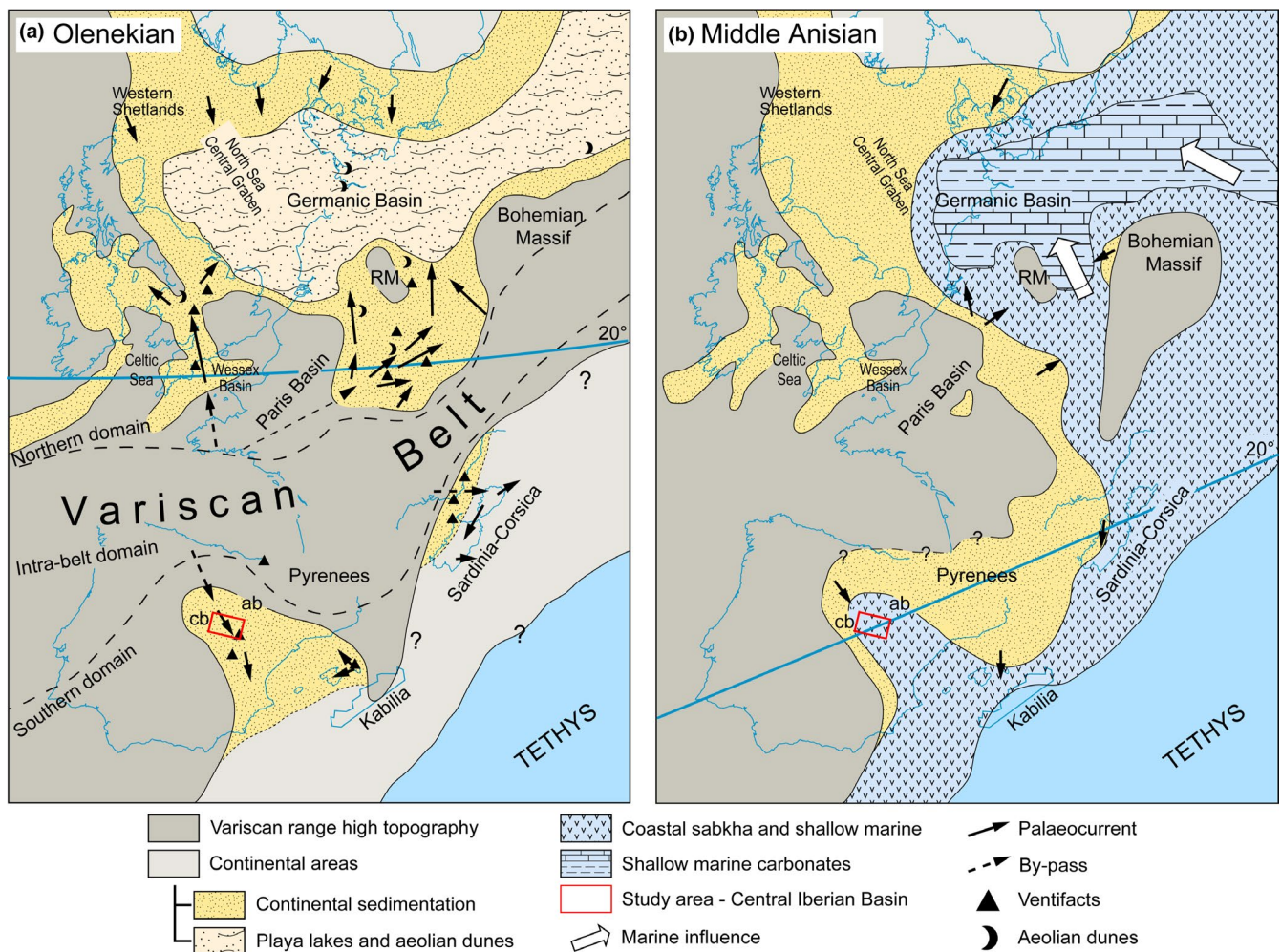


**FIGURE 2** Palaeogeographic reconstructions of the Olenekian (a) and Middle Anisian (b) of the north-western peri-Tethys domain. ab, Aragonian Branch; cb, Castillian Branch; RM, Rhenish Massif. Maps modified after Bourquin et al., 2011

the Muschelkalk (Bourquin et al., 2011; Muñoz, Ramos, Sánchez-Moya, & Sopena, 1992).

Detailed descriptions of the Permo-Triassic sediments have been made (see Arche & López-Gómez, 1999a, 1999b; Arche & López-Gómez, 1999; Arche, López-Gómez, Marzo, & Vargas, 2004; Borrueal-Abadía et al., 2015; Bourquin et al., 2011; Bourquin, Durand, Diez, Broutin, & Fluteau, 2007; Diez et al., 2010; López-Gómez & Arche, 1993a, 1993b; López-Gómez & Arche, 1993a, 1993b; López-Gómez & Arche, 1997; López-Gómez et al., 2002; López-Gómez et al., 2012; Ramos et al., 1986; Sopena et al., 1988; Van Wees, Arche, Beijdorff, López-Gómez, & Cloetingh, 1998). Formations throughout the basin were named differently according to their location along the NW-SE striking axis of the Iberian Ranges and specifically the Castillian Branch. To compare the sediments across the different localities, the formations have been correlated in time, and to the Germanic lithostratigraphic units, and are briefly summarised in the following (Figure 3). The

Boniches area was included to enable a correlation towards the south-eastern parts of the Iberian Ranges (Figures 1 and 3).

The Saxonian Facies include the Boniches Formation (BC), which is only found in the southeast, and is interpreted as alluvial fan deposits consisting of mainly conglomerates with a coarse sandy matrix and quartzites of up to 40 cm in diameter (López-Gómez & Arche, 1993, 1993b, 1997). A general fining upward trend can be related to the erosion of the source areas and a backstepping of the alluvial fans (López-Gómez & Arche, 1993a, 1993b). The Alcotas Formation (AMS) consists of fine-grained mud and silt intervals interbedded with lenticular sandstones and conglomerates. Sediment was deposited by braided fluvial systems with extensive floodplains and multi-story channel fillings (López-Gómez & Arche, 1993a, 1993b). The time-equivalent Montesoro Formation (MB) was deposited in the north-western part and comprises breccias, sandstones and siltstones with interbedded caliche profiles (López-Gómez et al., 2002).

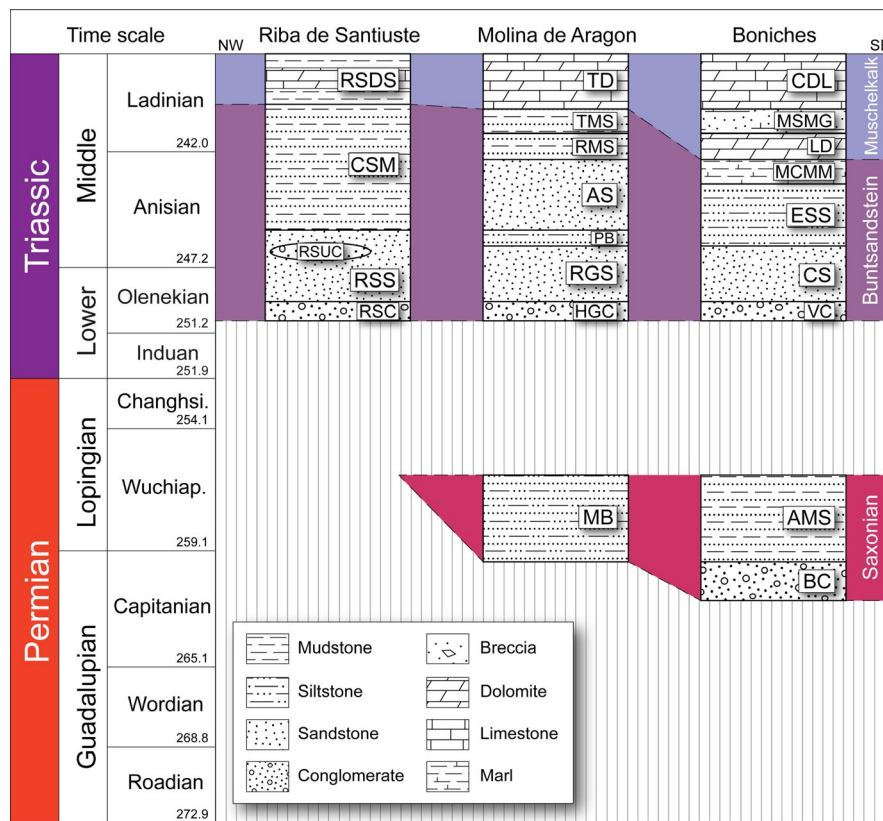


**FIGURE 3** Permo-Triassic lithostratigraphy of the Castillian Branch of the Iberian Ranges (after Arche et al., 2004; Diez et al., 2010; Ramos et al., 1986). The different lithological units in the Riba de Santiuste, Molina de Aragon (applicable for Riba de Saelices and Rio Gallo) and Boniches areas have been correlated with the Germanic Saxonian, Buntsandstein and Muschelkalk facies (López-Gómez et al., 2002). Abbreviations for formations are for Riba de Santiuste: RSC, Riba de Santiuste conglomerates; RSS, Riba de Santiuste sandstones; RSUC, Riba de Santiuste upper conglomerates; CSM, Cercadillo sandstones and mudstones; RSDS, Riba de Santiuste dolostones and mudstones; for Molina de Aragon: MB, Montesoro beds; HGC, Hoz de Gallo conglomerates; RGS, Rillo de Gallo sandstones; PB, Prados beds; AS, Arandilla sandstones; RMS, Rillo mudstones and sandstones; TMS, Torete mudstones and sandstones; TD, Tramacastilla dolostones; for Boniches: BC, Boniches conglomerates; AMS, Alcotas mudstones and sandstones; VC, Valdemeca conglomerates; CS, Cañizar sandstones; ESS, Eslida siltstones and sandstones; MCMM, Marines clays; marls and mudstones; LD, Landete dolomites; MSMG, Mas sandstones; marls and gypsum; CDL, Cañete dolomites and limestones. (ages after Ogg, Ogg, & Gradstein, 2016)

The Buntsandstein sedimentation started in the Early Triassic and comprises a range of different formations across the study area consisting mainly of continental, fluvial deposits (red beds). The Boniches area records a transition from basal conglomerates (Valdemeca Unit [VC]) to massive, medium-grained, red-pink sandstones (Cañizar Formation [CS]) deposited by sandy braided rivers. The top is marked by the Eslida Formation (ESS), consisting of red to pink arkoses and interbedded, massive mudstones, which were deposited by distal braided to high sinuosity streams.

Distinctive soil horizons with carbonate nodules indicate long periods of stability (López-Gómez & Arche, 1993a, 1993b). A similar sedimentary sequence is recorded in the Molina de Aragon and Riba de Santiuste area with alluvial fan/fluvial conglomerates at the base (Hoz de Gallo Formation [HGC] and Riba de Santiuste Conglomerates Formation [RSC]) overlain by medium-grained sandstones (Rillo de Gallo Formation [RGS], Arandilla Formation [AS] and Riba de Santiuste Sandstones Formation [RSS]) (Arche et al., 2004). The Molina de Aragon sequence is



**FIGURE 4** Photographs of the three key localities, where the detailed sedimentological study was undertaken. (a) Upper Buntsandstein section in Riba de Santiuste exposed in an eroded anticline with a bed dip of ~50 to 60 degree. (b) Lower Buntsandstein conglomerates and stacked, amalgamated sands of the Rio Gallo gorge. (c) Riba de Saelices area showing the complete Buntsandstein succession (Photo taken from DroneRS, 2019). Labelled units are shown in Figure 5

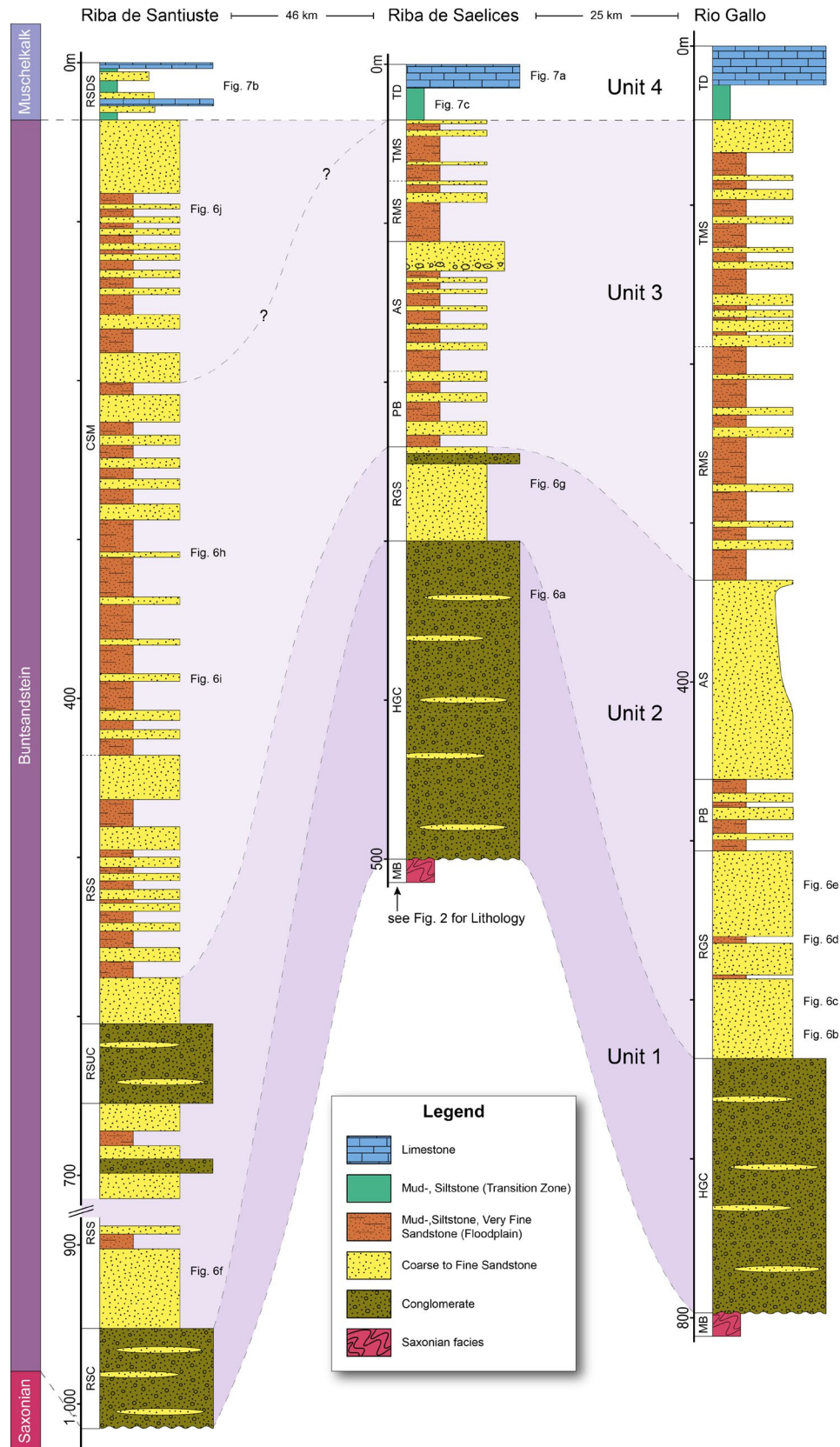


**FIGURE 5** Generalised graphic logs of the Buntsandstein facies of the three key localities Riba de Santiuste, Riba de Saelices and Rio Gallo. A correlation of the different interpreted lithological units is shown by the dashed lines. Each log is correlated using the transition from Buntsandstein to Muschelkalk sediments and started from the Saxonian (strongly red mud- and siltstones) to Buntsandstein boundary

interbedded with the more fine-grained sandstones and siltstones of the Prados Formation (PB). In Riba de Santiuste, the top and transition to the Muschelkalk unit is marked by interbedded, fluvial sand and silt/mudstones (Cercadillo Formation [CSM]).

The Muschelkalk unit in the CIB comprises the Marines Formation (MCMM) in the Boniches area, which is equivalent to the Germanic Röt Formation and records the first marine influence of the Tethyan transgression (Diez, Bourquin, Broutin, & Ferrer, 2007; Diez et al., 2010; López-Gómez & Arche, 1993a, 1993b). It consists mainly of dolomites, which change from lagoon carbonate mudstones to sabkha deposits showing transgressive–regressive cycles within the formation (López-Gómez et al., 2002). The overlying Landete Formation (LD), Mas Formation (MSMG) and Cañete Formation (CDL) consist of dolomites, limestones and evaporites and further emphasise the marine influence on the basin. Time equivalent in the areas to the northwest, the Rillo Formation (RMS) and Torete Formation (TMS) in the Molina de Aragon and the Fraguas Formation (FM) in the Riba de Santiuste area show a generally more continental influence with mudstones, evaporites and interbedded sand and siltstones (Figure 3).

### 3 | METHODOLOGY

The sedimentological analysis presented in this study focuses on three key localities (Figure 1b). Measurements of bed thickness and grain size and the determination of internal structures along profiles enabled the construction of graphic logs, which are used to document the sedimentary succession and to describe the fluvial architecture. Palaeocurrent analysis of sand bodies was carried out to infer palaeoflow directions of the ancient river system, and to determine the spatial arrangement of architectural elements within outcrops (Dasgupta, 2002; DeCelles, Langford, & Schwartz, 1983).

For the chemostratigraphic analysis, samples were collected predominantly from the centre of sandstone beds and at least 20 cm beneath any weathered surface. Sections were chosen from the key localities (Riba de Santiuste, Riba de Saelices and Rio Gallo), together with several profiles from selected intervening outcrops (Luzago, Ablanque and Ventosa, see Figure 1) to improve correlation across the basin.

The samples were prepared for geochemical analysis following Jarvis and Jarvis (1992a, 1992b); Pearce et al. (1999) and Pearce, Wray, Ratcliffe, Wright, and Moscariello (2005) and were analysed by Inductively-Coupled Plasma-Optical Emission Spectrometry (ICP-OES) and Inductively Coupled Plasma-Mass Spectrometry (ICP-MS), with quantitative data being acquired for 48 elements of which 10 are major oxides (Si, Ti, Al, Fe, Mg, Mn, Ca, Na, K and P), 24 are trace elements (Ba, Be, Co, Cr, Cs, Cu, Ga, Hf, Mo, Nb, Ni, Rb,

Sc, Sn, Sr, Ta, Tl, Th, U, V, W, Y, Zn and Zr) and 14 are rare-earth elements (La, Ce, Pr, Nd, Sm, Eu, Gd, Tb, Ho, Dy, Er, Tm, Yb and Lu). Precision error for the major oxides is generally better than 2% and is around 3% for the high abundance trace elements, whereas the data obtained from ICP-MS analyses generally are less precise (precision error ~5%), as the elements analysed by this method are present in very low concentrations that are close to the detection limits of the technique.

## 4 | SEDIMENTOLOGY OF THE TRIASSIC SEDIMENTS

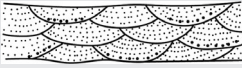
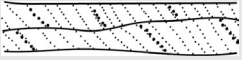
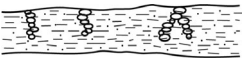
The studied sections were chosen as representative of the regional stratigraphy. They vary in thickness along the basin margin. Maximum thickness is about ~800 to 1000 m at the Riba de Santiuste and Rio Gallo sections (Figures 1 and 4). To the northeast, strata pinch out against a Palaeozoic intra-basinal high that compartmentalises the basin (Hall, 2005). Along the southern margin, normal fault segments have been interpreted and record synrift sedimentation (Hall, 2005).

The studied sections are comprised of two main lithologies, conglomerates and sandstones, with a lesser component of siltstones and/or mudstones. Various portions of the Permo-Triassic sediments have been described previously (see section ‘Geological Setting’), but this is the first time the complete synrift fill has been described from a fluvial system in the CIB. The following section characterises the sediments encountered at the key locations (Figures 4 and 5); lithofacies are described and summarised in Table 1. Four units are identified.

### 4.1 | Unit 1: conglomerates

The lower section of the Buntsandstein sediments is recognised by a succession of red to dark red conglomerates up to 200 m in thickness (Riba de Saelices area) with various arrangements of lithofacies Gp, Gt and Gms (Figures 5 and 6). The conglomerates can be clast or matrix supported depending on their depositional environment with predominately well rounded to sub-rounded quartzite clasts. Lateral accretion conglomerates show cross-bedding with fining-upward cycles of the individual beds (facies Gp). They are mostly clast supported with pebble to cobble clast size range (from 0.5 to 10 cm). Very coarse sand layers occasionally mark the top of one cross-bed set. Medium to coarse-grained sand lenses of 0.1–1 m in thickness interbed the conglomerates with variable frequency. Channel-fill conglomerates have a smaller clast size of up to 4 cm and are limited to the bottom and top by erosive surfaces. Throughout the lower succession, poorly sorted

**TABLE 1** Lithofacies classification used for the Permo-Triassic sediments of the Central Iberian Basin (after Miall, 1985, 1996)

Facies code	Facies description	Sedimentary structures	Interpretation	Thickness
<b>Gravelly lithofacies</b>				
Gp	Clast or matrix supported, red gravel with planar cross-stratification, clasts are mainly quartzites up to 10 cm in diameter, may show grading		Gravel bars	Individual beds: 0.5–1.5 m
Gt	Clast or matrix supported, red gravel with trough cross-stratification, clasts are mainly quartzites up to 10 cm in diameter, may show grading		Minor channel fills	Individual sets: 0.5–1.0 m
Gms	Massive, red gravel with horizontal bedding and clasts up to 25 cm in diameter		Longitudinal bars, lag deposits	Individual beds: 0.3–5.0 m
<b>Sandy lithofacies</b>				
St	Medium- to very coarse-grained sand, red, orange or pink colour, often includes pebble layers, may include rip-up clasts, trough cross-stratification		Sand dunes with sinuous crests, linguoid type (lower flow regime)	Individual sets: 0.2–0.8 m beds: 1.0–3.0 m
Sp	Medium- to very coarse-grained sand, red, orange or pink colour, often includes pebble layers, may include rip-up clasts, planar cross-stratification		Sand dunes with straight crests, sandwaves, bars (lower flow regime)	Individual beds: 1.0–3.0 m
Sh	Fine- to coarse-grained sand, red, orange or pink colour, may include pebble layers, horizontal lamination		Planar bed flow (lower and upper flow regime)	Individual beds: 0.5–2.5 m
Sr	Fine- to coarse-grained sand, red, orange or pink colour, ripple marks of variable size		Ripples (lower flow regime)	Individual sets: 0.2–0.5 m beds: 1.0–5.0 m
Ss	Fine- to coarse-grained sand, red, orange or pink colour, may include pebble layers, broad shallow scours, low-angle cross-stratification		Scour fills	Individual beds: 1.0–3.0 m
<b>Fine-grained lithofacies</b>				
Fl	Silt and mud with minor sand content, brown to red colour, fine lamination, high mica content, may be interbedded with fine-grained sand lenses		overbank or waning flood deposits	Individual beds: 0.2–10.0 m
Fm	Silt and mud with minor sand content, brown to red colour, massive, may show palaeosoils, desiccation cracks, bioturbation and colour mottles		Near channel deposits, vegetation cover	Individual beds: 0.2–2.0 m
Fr	Silt and mud with minor sand content, brown to red colour, massive, shows palaeosoils development with rhizoliths, may show calcareous glaebules		Near channel deposits, vegetation cover, increased maturity	Individual beds: 0.2–0.5 m
<b>Heterolithic lithofacies</b>				
Hms	Fine- to medium-grained sand lenses (yellow) interbedded with mud and silt (dark red to green), laminated		Estuarine, shoreface	Individual lenses: 0.1–0.5 m beds: 1.0–3.0 m
Hsc	Fine- to medium-grained sand with high carbonate content, white or greyish colour, massive, may show bedding surfaces		Beach, offshore bar/shoal	Individual beds: 1.0–2.0 m

(Continues)

TABLE 1 (Continued)

Facies code	Facies description	Sedimentary structures	Interpretation	Thickness
Hm	Mud with minor silt content, grey to dark green colour, fine lamination, may show minor fine-grained sand lenses, and gypsum layers		Supratidal deposits, intertidal mud flat	Individual beds: 0.2–0.5 m
Hsr	Very fine- to fine-grained sand with silt, yellow to red colour, bioturbation ( <i>Diplocraterion</i> , <i>Skolithos</i> ), wave and linguoid ripple marks		Tidal/intertidal flat	Individual beds: 0.2–0.5 m

conglomerate beds with up to 5 m thickness can be found (Gms). They are matrix or clast supported and have a clast size of up to 25 cm in some matrix-supported beds. There is little sedimentary structure noticeable and the lateral extent often reaches beyond the exposure (>50 m). The top of unit 1 is marked by an interbedding of matrix-supported conglomerates and sheet-like, red sandstone beds (Figure 6a).

With palaeocurrent directions spanning 040 and 130 degrees, roughly perpendicular to the NW-SE basin axis, the basal conglomerates are interpreted to have been deposited as proximal fan systems running down the south-western rift shoulder of the basin. Large-scale coarsening-upward sequences within the conglomerate succession further emphasise an alluvial fan system as the depositional environment with fan-lobe growth as the primary control on grain size (Ramos et al., 1986, their figure 13d). Further towards the top of unit 1 palaeocurrents change towards the southeast (090–130 degrees), suggesting a shift to the establishment of a basin axis parallel stream flow-dominated drainage system, which is fully developed in the overlying units.

#### 4.2 | Unit 2: stacked, amalgamated sandstones

With the onset of the sand-dominated unit (Figure 5), the palaeoflow direction of the system consolidated to the southeast. The sediments are characterised by medium to coarse grained, pink to red fluvial sandstones (facies St, Sp, Sr and minor Ss, Figure 6b,c). In places, sandstone dune bedforms with straight crests are preserved and visible in 3D (Figure 6c,e). Amalgamated sandstone packages reach a thickness of up to 50 m and are built of internally stacking channel sands with basal scours and erosive contacts to older deposits. Small-to-medium pebbles are found throughout the sediments and are often aligned parallel to foreset laminae. Overall grain size is fairly constant within the sandstone beds, but shows fining upward sequences on a cross-bed-scale or within small-scale channel features. In places, cobbles of mainly quartzite accumulate at the scour base of a channel fill and decrease in abundance upward within the fill.

In the Rio Gallo area, several distinct flood plain horizons are recognised (Figure 6d). They are up to 4 m thick and comprised of dark red siltstone with minor sand content (facies Fl, Fm). The presence of rhizoliths up to 15 cm in length indicates soil formation and sparse vegetation cover on the flood plains. Pedogenic features could not be observed at the localities to the northwest.

In the Riba de Santiuste area, a ~50-m-thick conglomerate succession (facies Gms) with internal coarse-grained sandstone lenses is interbedded with the stacked sandstones towards the top of the unit. A possible reason is a short-lived fan system, due to the proximity of the region to the basin margin and rift shoulder, triggered by local tectonic activity at the main boundary fault.

The deposits of unit 2 are interpreted as sandy-braided river deposits. The system was characterised by relatively short-lived channels with low stability undergoing strong lateral migration and avulsion. This resulted in the complex geometry of the internal channel stacking patterns and amalgamation. The absence of preservation of significant amounts of mud in the system within this unit suggests little accommodation space availability and generally an overfilled basin state.

#### 4.3 | Unit 3: isolated sandstones

Unit 3 is marked by an increase in floodplain facies abundance resulting in isolated sandstone beds and partly amalgamated complexes, but also single-storey bodies (Figure 6h,i). The lower section of this unit is recognised by tabular, sheet-like, pink to red sandstone bodies with a thickness ranging between 2 and 5 m and extending laterally for 50–100 s of m, often beyond exposure (Sp, Sh, Ss, and minor St). Several vertically and laterally stacking sand bodies, which erode into older units, often build the isolated sand bodies. Grain size ranges from medium to coarse sand with fining upward sequences within the individual bodies (Figure 6f,g). The base often incorporates pebbles and cobbles up to 4 cm in diameter.

Floodplain facies of very fine sand to silt separate the individual sand beds or amalgamated complexes and reach up to 20 m in thickness (facies Fl). These beds are dark

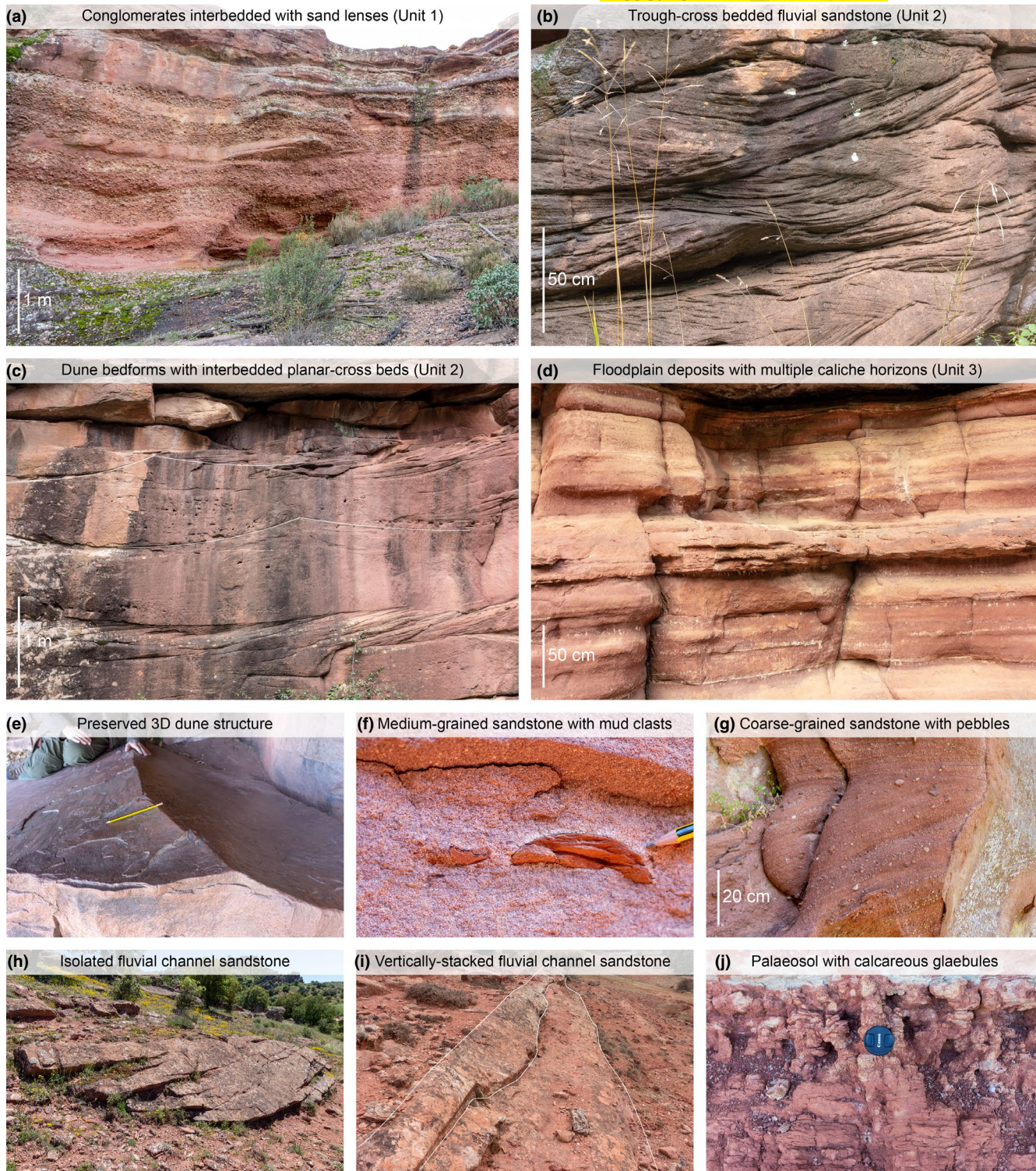


**FIGURE 6** Photographs of different sediments corresponding to different fluvial styles and facies of the Triassic Buntsandstein in the Castillian Branch of the Iberian Ranges. (a) Conglomerates of unit 1 (FIGURE 5) in the Riba de Saelices area interbedded with coarse- to very coarse-grained sandstone beds. (b) Trough cross-bedded sandstones of unit 2 in the Rio Gallo area as part of an amalgamated complex. (c) Stacked sandstone bodies in the Rio Gallo area of unit 2 showing planar cross-bedding and dune bedforms. (d) Floodplain deposits in the Rio Gallo area of unit 3. Multiple caliche horizons are interbedded with silt to very fine-grained sandstones. (e) Exposed dune bedform as seen in (c) in the Rio Gallo area. The pen for scale is 15 cm. (f) Medium-grained sandstone with mud clasts in the Riba de Santiuste area. Note pen tip for scale. (g) Coarse-grained, planar cross-bedded sandstone with pebbles up to 4 cm in diameter. (h) Ribbon-shaped fluvial sandstone body isolated by floodplain sediments in the Riba de Santiuste area. The sandstone body is ~2 m in thickness. (i) Sheet-like channel body (2.5 m thick) with internal channel stacking and scouring with low-angle cross-bedding and a fining upward sequence within the individual beds. (j) Palaeosol with calcareous glaebules in the Riba de Santiuste area. Lens cap is 6.7 cm in diameter

red in colour, finely laminated and commonly include a high mica content. Crevasse splays within the floodplain sediments are represented by 10–50 cm thick very fine to fine sandstone sheets or lenses, which extend laterally up to 50 m. The top of these floodplains are frequently recognised by dark red to red muddy/silty palaeosols with calcified rhizoliths, superficial or very shallow trace fossils such as living burrows and feeding trails and colour mottling from dark red to medium grey (facies Fm). Further towards the top of the Buntsandstein unit, the palaeosols are formed by calcareous nodules (Figure 6j) showing an increased bank stability, longer-term channel existence and favouring sinuosity (Fr). This upper section is characterised by the tendency of the sand bodies to form increased amalgamated complexes of 5–25 m in thickness. Minor isolated sandstone beds with a thickness of 2–5 m show a fining upward from coarse to medium/fine-grained sandstone on the top. Lateral accretion surfaces interpreted as point bars can also be found in these deposits. The beds have a sheet-like or lenticular shape and extend laterally for more than 100 m, often limited by outcrop exposure. The scoured, irregular bases often incorporate pebbles, which are in places aligned in palaeoflow direction.

The architecture and thickness of unit 3 differ in the Riba de Santiuste area from the locations to the southeast. Here, the deposits reach a greater thickness of ~550 m and are characterised at the top of the unit by a ~40-m-thick amalgamated complex (facies Sp, St, Ss). Floodplains in the upper section of this unit are more abundant, thicker and show an increased formation of calcareous glaebules (Fr).

An increase in channel stability and sinuosity is recognised towards the top of the Buntsandstein section in this unit (especially in the Riba de Santiuste area, but also in Rio Gallo). There is evidence for the fluvial system shifting from predominantly braided (Unit 2) to a more meandering style system at the top of unit 3. This is supported by lateral accretion surfaces in the isolated sandstones and the advanced development of palaeosols on the floodplains. The high preservation of fine-grained lithologies can be explained by an increased subsidence rate creating abundant accommodation space favouring the deposition of floodplain, overbank and palaeosol fines.

#### 4.4 | Unit 4: carbonates and calcareous sandstones

The top of the studied section is marked by the marine sediments of the Muschelkalk, which is also used as a correlation surface in the basin (Figure 5, Unit 4, Figure 8). The Tethys ocean transgressed over the Iberian Basin approaching the study area approximately from the southeast (Figures

1 and 2b). In the Rio Gallo and Riba de Saelices areas, the fluvial sedimentation of sandstones and siltstones stops fairly abruptly and changes to interbedded, very fine to fine-grained sandstone with mud and siltstone (facies Hms, Hm) (Figure 7c). The thickness of the individual beds varies from 5 to 30 cm and sandstone content decreases towards the top. This 'transition zone' from continental to marine sedimentation also includes minor gypsum horizons (thickness between 2 and 4 cm) within the mudstones (Figure 7h), which are indicative of a periodical evaporation of sea water and a nearshore interplay of short-term marine transgression and regression. Marine sedimentation fully takes over after the thickness of this heterolithic zone had reached 20–30 m. This is recognised by bioclastic limestones and dolomites, which form distinctive cliffs of 15–30 m in height (Figure 7a). Early carbonate deposits show an increased amount of mud and sand content. Mud/sand content reduces towards the top of the unit producing cleaner carbonates.

The transition from fluvial to marine sedimentation in the Riba de Santiuste area (Figures 2b and 8b) in the northwest of the study area follows a different sedimentary pattern. Here, an extensive 'transition zone' and thick, blocky carbonates are absent. Instead, calcareous sandstones (calcarenes, Hsc) reach a maximum thickness of ~8 m and strongly vary in carbonate content (Figure 8g,i). This is succeeded by mudstone with fine sand stringers (Hm) and topped by ~6 to 8 m of silt and sand with distinct ripple marks and bioturbation of *Skolithos* and *Diplocraterion* indicating a dynamic, high-energy environment (facies Hsr) (Figure 7d–f). Fine-grained, clean carbonates of 10–20 cm in thickness mark the top of the succession.

The sedimentation at Riba de Santiuste shows a more pronounced interplay of continental and marine strata than at the locations to the southeast where marine deposits are dominant. This can be explained by a decreasing magnitude of the marine transgression at this point with the preservation of potential beach and tidally influenced sediments, which are not observed in the south-eastern part of the basin. A thicker succession of shallow marine to estuarine muds further emphasises a slowing of the transgression and longer-lived establishments of near-shore environments. The reduced thickness of carbonates is indicative of the transgression reaching its landward limit of progradation.

## 5 | CHEMOSTRATIGRAPHIC CORRELATION

The chemostratigraphic analysis was undertaken along six profiles of the Triassic Buntsandstein sediments (Figure 1b). Element ratios (Figures 8 and 10) show vertical variations within each profile which can be used to correlate sequences between the profiles across the study area. Plots are

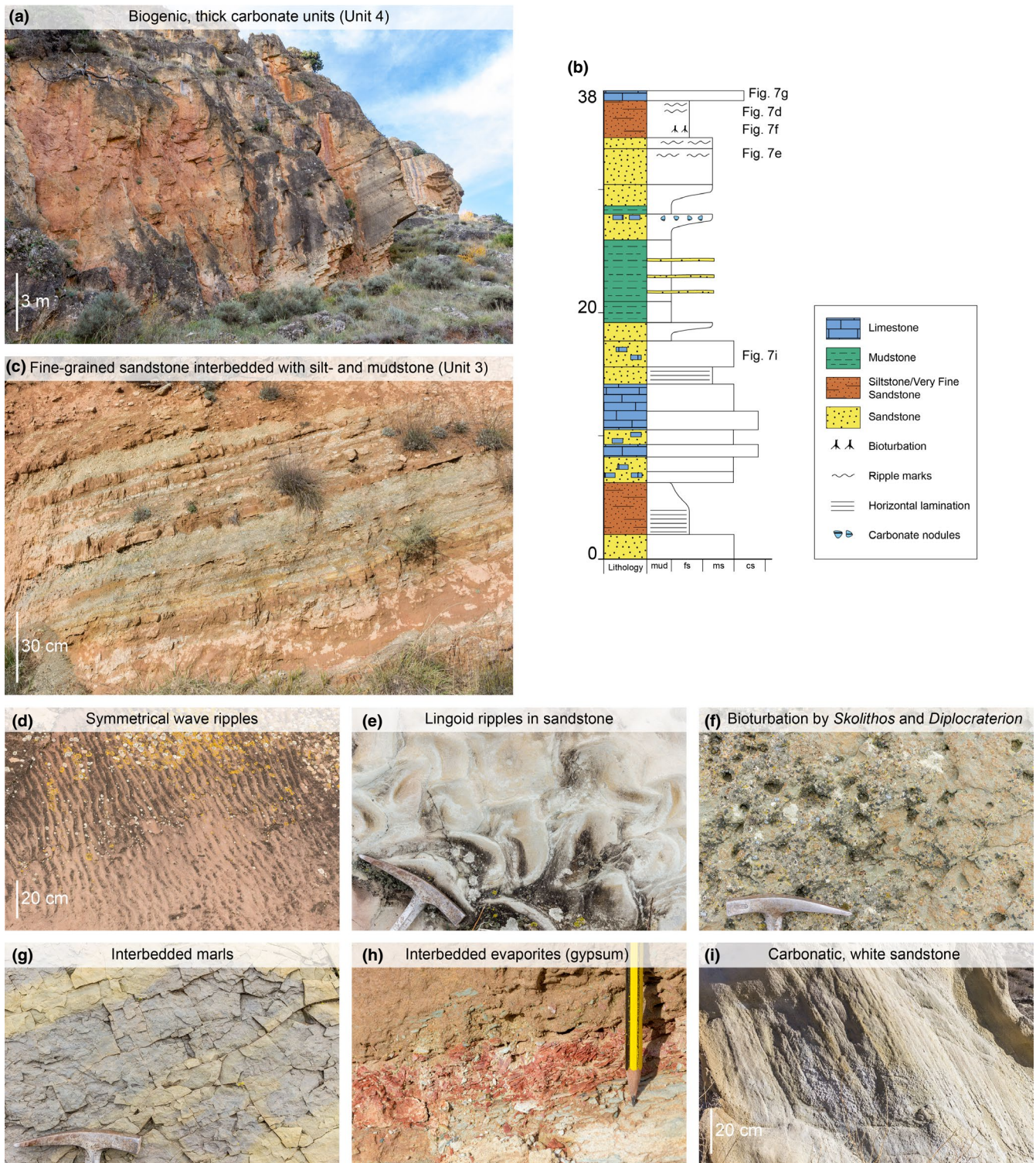


**FIGURE 7** Photographs of the transition to and carbonates of the Muschelkalk facies in the Castillian Branch of the CIB. (a) Cliffs of biogenic carbonate of the Muschelkalk facies in the Riba de Saelices area. (b) Graphic log of the Buntsandstein to Muschelkalk transition in the Riba de Santiuste area. Note the absence of thick carbonate units as seen at the other locations. (c) Interbedding of sandstones and mud/siltstones in the transition zone to the Muschelkalk facies in the Riba de Saelices area. (d) Symmetrical wave ripples in silty, very fine-grained sandstone in the Riba de Santiuste area. (e) Linguoid ripples in silty, very fine-grained sandstone in the Riba de Santiuste area. Hammer for scale is ~18 cm. (f) Bioturbation by *Skolithos* and *Diplocraterion* in mud-rich siltstone in the Riba de Santiuste area. Hammer for scale is ~18 cm. (g) Marls interbedded in the uppermost section in the Riba de Santiuste area. Hammer for scale is ~18 cm. (h) Interbedded layer of evaporate deposits (gypsum) in the Riba de Saelices area. Note pen tip for scale. (i) Carbonate-rich sandstone (calcarenite) with horizontal lamination in the Riba de Santiuste area. The beds are dipping ~60 degrees

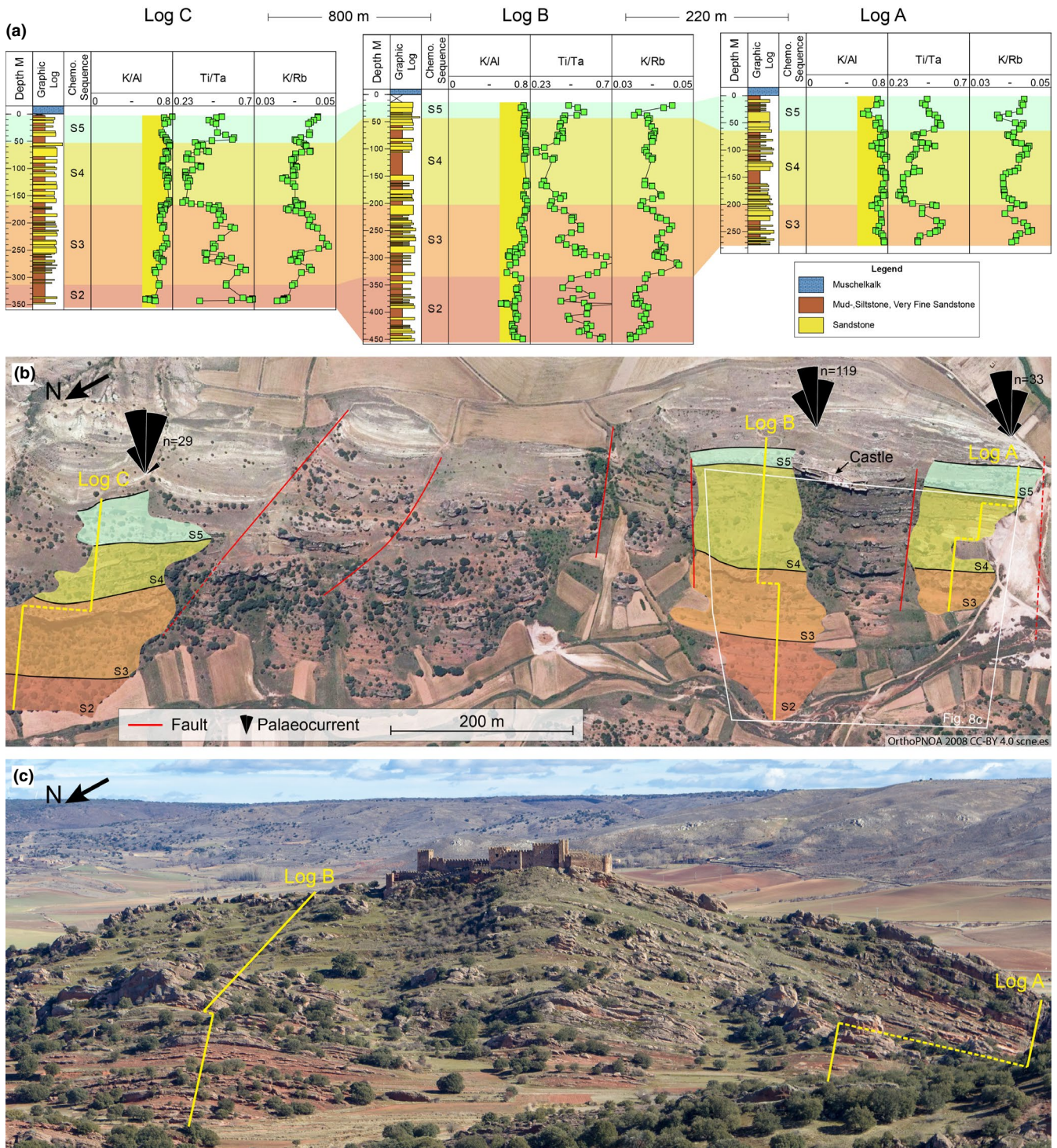


**FIGURE 8** (a) Chemostratigraphic profiles in the Riba de Santiuste area (Location indicated in Figure 1) showing K/Al, Ti/Ta and K/Rb element ratios and interpreted chemostratigraphic sequences. (b) Satellite image of the eastern flank of the Riba de Santiuste anticline. The location of the chemostratigraphic profiles is indicated by the yellow lines. The indicated palaeocurrent directions are situated next to the log locations where they were measured. (c) Photograph of the castle section in Riba de Santiuste showing the location of chemostratigraphic profiles A and B. The castle for scale is ~90 m wide

normalised to  $Al_2O_3$  to minimise the influence of grain size effects on the geochemical composition of the sandstones. The element ratios of K/Al, Ti/Ta and K/Rb of the sandstone chemistry were used as the main correlation elements as they

were found to be the most useful and consistent throughout the chemical dataset yielding the best results for robust correlation. Vertical changes in elemental compositions can be clearly recognised in the study sections (Figures 8 and 9).

Changes in sediment provenance with associated changes in the sediment composition, and effects of weathering during deposition are considered in all correlation profiles (Ratcliffe et al., 2015). In this section, the detailed correlation of the studied sections is appraised.

## 5.1 | Correlation of strata at outcrop scale

The nature of the outcrops at Riba de Santiuste enables an investigation of the development of the fluvial system which is exposed in an eroded anticline over a length of ~1.4 km roughly perpendicular to palaeoflow direction (Figures 4a and 8). Three chemostratigraphic profiles were collected to correlate the fluvial facies laterally along the outcrop. The logs are situated in the upper Buntsandstein section and end with the start of the Muschelkalk (Units 3 and 4 in Figure 5).

A good correlation of the chemostratigraphic profiles overall is achieved between the three profiles (Figure 8a). Sequence S2 is only recognised in log C and B due to better exposure at those localities. Ti/Ta and K/Rb values increase towards the top of the sequence in the profiles and indicate the start of sequence S3, which is found in all profiles. This sequence is ~150 m in thickness and only partly recognised and exposed in log A. Sharply decreasing Ti/Ta and K/Rb values in all three profiles are interpreted as the top of sequence S3. Sequence S4 is characterised throughout by high K/Al values and initially low Ti/Ta and K/Rb values that

steadily increase towards the top of sequence S4 in all profiles. The start of top sequence S5 is interpreted by a sharp increase in Ti/Ta and K/Rb values and a decrease in the K/Al ratio. After the initial decrease, the Ti/Ta and K/Rb ratios decline until the end of the profiles, which is recognised by the start of Muschelkalk sediments.

Several faults crosscut the flank of the anticline and offset the fluvial sediments. Attempting to correlate the fluvial deposits according to the individual architecture of the beds is particularly challenging due to their inherent variability (Figure 8b,c). However, chemostratigraphy is decoupled from the fluvial architecture as it reflects the elemental sediment composition, which is controlled predominantly by sediment source areas and climate-induced weathering. Chemostratigraphy provided a more robust technique for correlation of the fluvial stratigraphy.

## 5.2 | Correlation of strata at basin scale

The chemostratigraphic correlation was extended to cover a length of ~80 km along the south-western margin of the CIB. At six locations, geochemical profiles of the Buntsandstein sediments were investigated and correlated according to their chemical composition (Figure 9). The studied profiles can be divided into five distinct sequences (S1–S5) based on trends in element ratios. Not all sequences were observed at every location due to incomplete sections.

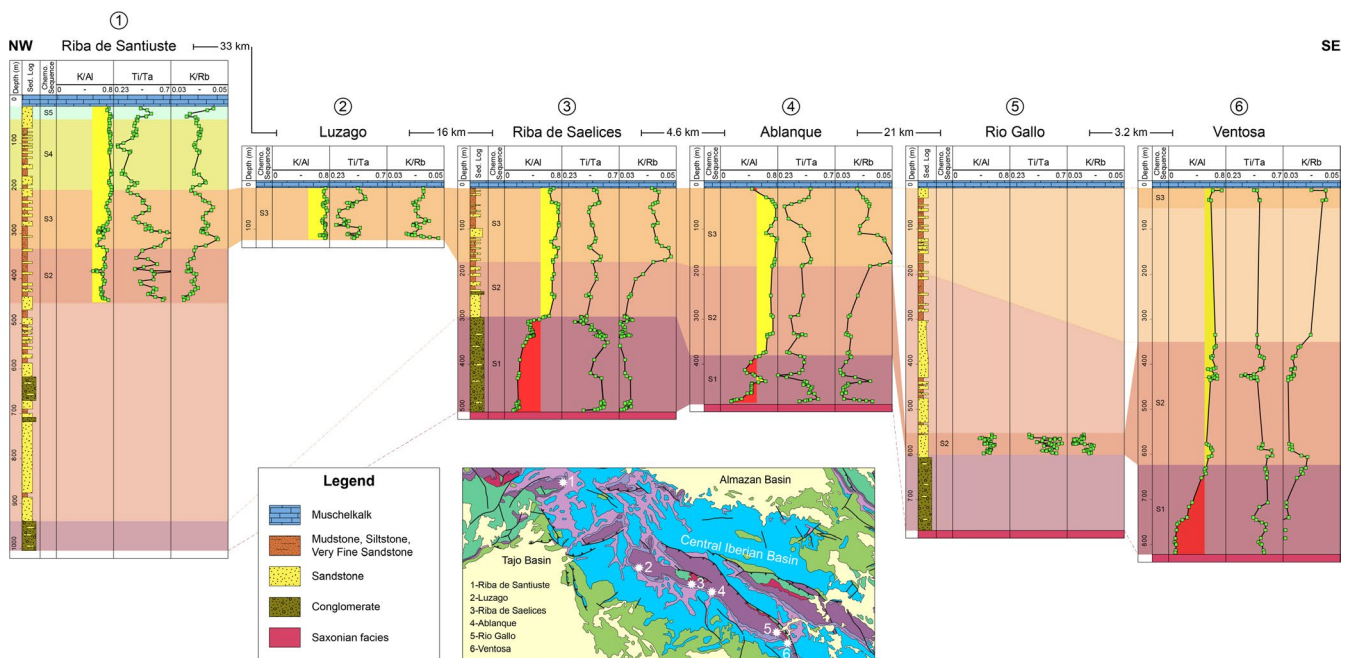


**FIGURE 9** Chemostratigraphic profiles of selected outcrops along the south-western margin of the CIB. The profiles have been correlated using trends in K/Al, Ti/Ta and K/Rb element ratios. A sedimentary log for the key locations is shown to highlight relationships between sedimentary architecture and chemostratigraphic signature of the sediments. Areas of unavailable data at Riba de Santiuste are shown in white and at Rio Gallo and Ventosa those areas are interpreted with paler colours of the related sequence. The inset map shows the location of the chemostratigraphic profiles

Sequence S1 occurs in the Riba de Saelices, Ablanque and Ventosa profiles and is described by lower K/Al ratios and higher Ti/Ta ratios than the overlying sequence. Ti/Ta ratios decrease towards the top boundary of this sequence. K/Rb ratios are generally lower than the succeeding sequence. This sequence is the only one throughout the basin succession that correlates with sedimentary unit 1, the basal conglomerates. It could be inferred that the conglomerates succession at the base at Rio Gallo is of a similar chemostratigraphic signature.

Sequence S2 spans across the whole study area, except the Luzago area. It is differentiated from the underlying sequence by higher K/Al ratios and a trend of increasing K/Rb ratios towards the top of this sequence. Ti/Ta ratios show generally medium values, but are subject to higher variations in Riba de Santiuste and Rio Gallo, which might be attributed to an effect of the higher sample density in this sequence compared with the other locations.

Sequence S3 can be observed in all geochemical profiles except the Rio Gallo area. It shows similar K/Al ratios to sequence S2, but is differentiated by higher K/Rb ratios at the base that decline towards the top of the sequence. The sharp increase in Ti/Ta ratios at the base of the sequence further emphasises the lower boundary. In Ventosa, data are available for the uppermost sections, but we infer that the resulting gap is part of sequence S3. The profile at Luzago was collected from the Muschelkalk to the basement, thus represents the complete Triassic basin infill at this location with the chemical signature corresponding to sequence 3. The reduced thickness at Luzago can be explained by sediment bypass and/or low accommodation space.

The succeeding sequences S4 and S5 are only observed in the Riba de Santiuste area and described in detail in section 5.1. The main difference and reasons for interpretation of those separate sequences is the drop in Ti/Ta and K/Rb ratios and the generally lower values of both ratios (especially Ti/Ta) compared with other locations. In addition, the sharp increase in both ratios observed at the top of the successions is unique to this location.

The chemostratigraphic correlation reveals an additional section of ~200 m of fluvial sediments in the Riba de Santiuste area with a unique elemental signature (Table 2).

## 6 | PRINCIPAL COMPONENT ANALYSIS

To infer on element configurations and the related minerals controlling those elements, a principal component analysis (PCA) was conducted, which is widely used in chemostratigraphy (Ellwood et al., 2008; Pe-Piper, Triantafyllidis, & Piper, 2008; Ratcliffe et al., 2015; Sano, Ratcliffe, & Spain, 2013; Svendsen et al., 2007). PCA reduces the amount of variables in a dataset, e.g. element concentrations, and expresses this variation by principal components (PC1, PC2). A score for each element concentration in relationship to the principal components is calculated and visualised in a loadings plot (Figure 10).

Elements tend to plot in clusters meaning that they are closely related to each other and potentially incorporated in the same mineral (Ratcliffe et al., 2015). The distance the elements plot from the origin (0, 0) of the plot indicates the influence on the principal variance, where a greater distance results in a higher influence. Centred log ratio transformation was applied to the original dataset before running the PCA to remove constraints, which could have an impact on the multivariate analysis.

By comparing the PCA analysis of the sandstones of the Riba de Santiuste section with the CIB one, it can be seen that the element group in similar clusters, except some minor differences. This primarily shows that the variation in the dataset is constant for the Riba de Santiuste section and basin-wide, meaning potentially similar element compositions basin-wide delivered by the same hinterland source area. Thus enabling a basin-wide correlation which is undisturbed by local sedimentary effects, e.g. local sources of sediment or different hinterland source areas supplying sediment to different parts along the western basin margin from late Permian–Early Triassic to Middle Triassic (~10 Ma).

**TABLE 2** Comparison of chemostratigraphic sequences and sedimentary units

Chemostratigraphic sequence	Sedimentary unit	Interpretation	Comment
S5	3	Fluvial sandstones and floodplains	Only observed in Riba de Santiuste
S4	3		Only observed in Riba de Santiuste
S3	2,3		
S2	2, 3		
S1	1	Basal conglomerate succession	

## 7 | DISCUSSION AND IMPLICATIONS

Changes in elemental chemistry have been used to define stratigraphic correlations between wells in many sedimentary basins. Few publications, however, relate defined chemical stratigraphy to physical correlations, and only limited numbers have been undertaken at a complete basin scale (e.g. Ratcliffe et al., 2015). The data presented above show that systematic trends occur in element ratios in a succession of complex fluvial strata and that these are laterally extensive, allowing robust correlations to be made along a basin margin. Furthermore, these correlations mimic physical chronostratigraphic correlations over short ~2 to 8 km and basin scale ~70 to 80 km distances, so that

in this study, chemostratigraphy provides robust chronostratigraphic correlations for basin-wide correlations. The use of chemostratigraphy has clearly identified a major single fluvial system connecting the studied locations along the margin of the CIB. Based on the detailed correlation of correlatable units in this study, chemostratigraphy provides a powerful tool for establishing basin-wide relationships in complex depositional environments and in particular where there are diachronous facies that have limited biostratigraphic controls.

However, it is apparent that the dynamic fluvial processes that control the deposition of the fluvial sediments and resulting sedimentary architecture can present some challenging correlations at the local scale (100's m to a few km). Changes between logged sections where there are no

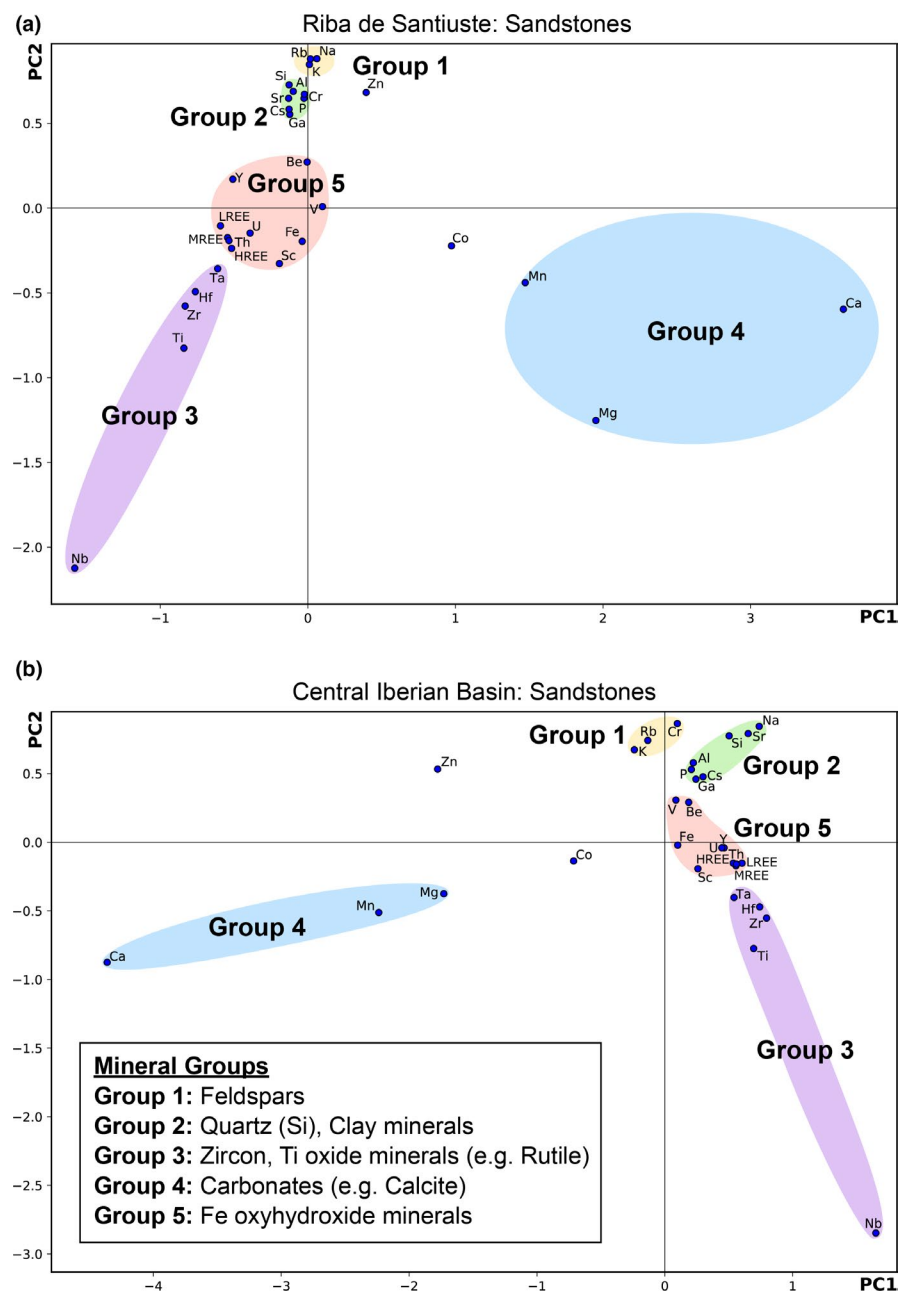


**FIGURE 10** Principal component analysis of elements for principal component 1 (PC1) versus principal component 2 (PC2). A comparable variation in both datasets indicates a similar element compositions basin-wide delivered by the same hinterland source area and thus a single fluvial system. (a) Principal component cross-plots of elements for the sandstones in Riba de Santiuste. (b) Principal component cross-plots of elements for the sandstones across the studied, south-western basin margin. HREE, heavy rare-earth elements (Ho, Er, Tm, Yb, Lu); LREE, light rare-earth element (La, Ce, Pr, Nd, Sm); MREE, middle rare-earth elements (Eu, Gd, Tb, Dy). All major elements are shown in an abbreviated form, e.g. SiO = Si, Al<sub>2</sub>O<sub>3</sub> = Al etc

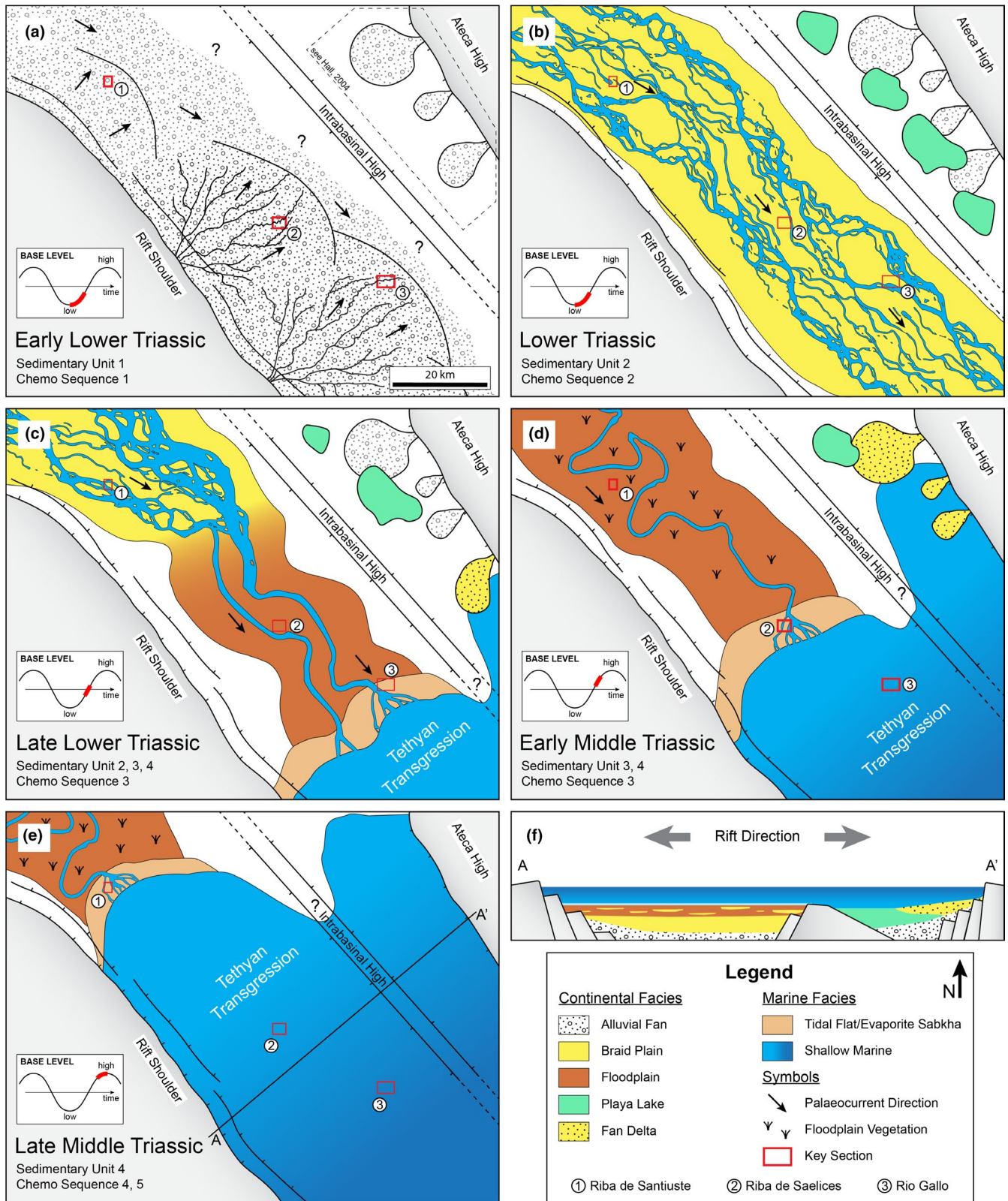


**FIGURE 11** Palaeogeographic reconstruction of the basin across the study area. (a–e) show the development of the fluvial system and the flooding of the basin by the marine transgression of the Tethys Ocean from the earliest Triassic to the Middle Triassic (Late Ladinian). In addition, the development of alluvial fans, playa lakes and fan deltas is shown in the northeast on the flank of the Ateca High. A suggested intrabasinal high is separating the fluvial system in the southwest from the sedimentation in the northeast. (f) Idealised cross-section (A–A') through the basin showing the synrift infill architecture and rift direction. Location is shown in (e). Inset schematic base-level graph identifies the role played by the Tethyan transgression and in (a) and (b) refer to relative sea level and not a tectonic base level during Early to Middle Triassic rifting phase

obvious field-based architectural similarities or grain size variations have been correlated using the strength of the element and elemental ratio characteristics (Figure 9), but at many sites similarities in channel architecture and stacking patterns over several 100's metres do not yield any obvious robust correlation. It is apparent that although field-based correlations have benefits for understanding allocyclic controls upon sedimentation (e.g. Bourquin, Guillocheau, & Péron, 2009; Bourquin, Péron, & Durand, 2006; Bourquin, Rigollet, & Bourges, 1998; Heller & Paola, 1996; Jones, Frostick, & Astin, 2001; Leleu, Lanen, & Hartley, 2010) and stacking pattern relationships (e.g. Colombera, Mountney, & McCaffrey, 2015; Flood & Hampson, 2017; Shanley & McCabe, 1994), two similar sand-dominated channel fills may differ in age, and their mineralogical composition reflect the composition of sediment that arrived at that position at different times. Thus, different positions within the channel belt and along its upper surface are diachronous, and this will be reflected as noise in the chemostratigraphic profile. Caution needs to be taken with the scale of the correlations used when applying chemostratigraphy and in this study correlations provide the most robust correlations of fluvial strata at the scale of >1 km. This has important implications for high-resolution correlation of fluvial strata in the subsurface where it may not always be clear as to what fluvial sand body can be correlated.

## 7.1 | Correlation of fluvial strata along a syntectonic basin margin

Synrift successions preserved in extensional basins record the interaction between rates of fault-controlled subsidence and sediment supply, and fluctuations in relative sea level (e.g. Frostick & Reid, 1989; Gawthorpe, Fraser, & Collier, 1994; Hall, 2005; Leeder & Gawthorpe, 1987; Prosser, 1993; Schlische, 1991). A number of papers have examined the role that fault segment interaction and linkage play in controlling the overall stratigraphic architecture, rate of subsidence and depocentre-migration patterns of rift basins (e.g. Anders & Schlische, 1994; Contreras, Anders, & Scholz, 2000; Gupta, Underhill, Sharp, & Gawthorpe, 1999; Jones, 2004; Young, Gawthorpe, & Sharp, 2002). Similarly, the sedimentation of fluvial stacking patterns and changes in architectural styles from early to late synrift phases have been widely examined (e.g. Gawthorpe & Leeder, 2000) and it has been shown that local depocentres adjacent to rift border faults record displacement maxima-focused channel stacking and allowed the aggradation of thick successions of fluvial strata (Davies, Dawers, McLeod, & Underhill, 2000). However, this aggradation of fluvial stacking is often confined to active short-lived faults with limited fault length of a few kms during the early synrift phase (e.g. Davies et al., 2000; Frostick &

Jones, 2002). We propose that the coarse conglomerate sediment dispersal was initially focused in evolving relay zones, and preferentially preserved adjacent to fault segment centres and this inference is supported by changes in palaeocurrents during the earliest phase of large alluvial fan Buntsandstein deposition. Similar occurrences have been noted for the northern margin of the CIB where relay zones along the northern border faults played a critical, if short-lived role, in the sediment supply (Hall, 2005). Overlap, interference and linkage of segments during fault evolution led to drainage reorganisation and the dominance of a major axial flowing river system. As episodes of fault growth and linkage are unlikely to occur simultaneously along the entire evolving border fault array of the CIB, then accommodation space must have outpaced the sedimentation rates certainly during the earlier phases of fluvial deposition and is evidenced by the robust chemostratigraphic correlations that indicate fairly consistent thickness along the entire margin of the basin (Figure 9, Sequence S1).

High sedimentation rates for the conglomerate section (Unit 1) resulted in a rapid infill of the initial synrift generated accommodation space. The conglomerates were derived primarily from the nearby rift shoulder with short transportation distances and high energy currents, e.g. flash flood and/or ephemeral fluvial sedimentation as part of a series of large alluvial fans (Figure 11a). The accommodation space available for the deposition of the subsequent high net to gross, stacked sandstone succession (Unit 2) was reduced and the basin was in an overfilled state as fine-grained lithologies are absent or only sparingly preserved locally (Figure 11b,c). This can be accounted for by either a period of slow rifting and steady sedimentation rates or an increased sediment supply outpacing the accommodation space without respect to rate of rifting and fault-controlled subsidence.

The preservation of fine-grained, floodplain sediments in the upper Buntsandstein succession (e.g. Riba de Santiuste section, Unit 3) supports a diminishing basin subsidence rate and a lowering of the basin floor gradient between the fluvial and encroaching marine system (Figure 11c–e). Furthermore, the ancient river system seems to have become more stable and increased in sinuosity up section, even meandering in the uppermost parts of the section (Figure 11d,e, Unit 3). This increased stability is favoured by a changing climate in the basin caused by the Tethyan marine transgression. Regular precipitation periods and, in general, a wetter climate resulted in vegetation growth on the floodplains thus increasing bank stability and sinuosity (Borrueal-Abadía et al., 2015; López-Gómez et al., 2012; Preto, Kustatscher, & Wignall, 2010). A wetter climate is supported by the Pangaeon monsoonal circulation, which reached its maximum strength during the Triassic and counts as a major factor for the continent-wide increase in precipitation from the Permian to the Early Triassic (Parrish, 1993).

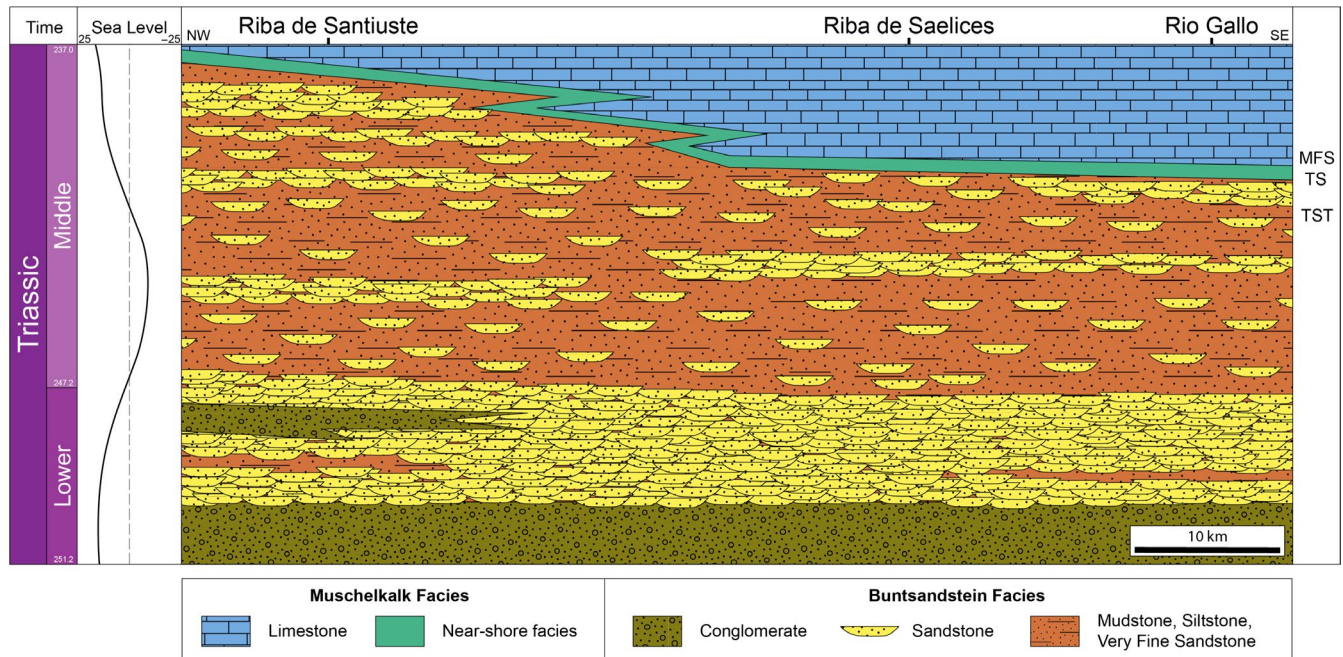


**FIGURE 12** Summary chart showing the development of the fluvial architecture at the key localities with relationship to approximate geological time. In addition, the sea level curve for that time interval is shown (after Haq, 2018)

In general, accommodation space was outstripping sediment supply in the early synrift stages and diminished through time resulting in an increase in sinuosity accompanied by a decrease in slope before the final marine flooding surface. The initial high accommodation space controlled the positioning of the fluvial system and was later maintained along the southern margin of the CIB (e.g. Peakall, Leeder, Best, & Ashworth, 2000). A proposed intrabasinal high further contributes to the positioning along the southern basin margin. This topographic structure can be inferred due to the absence of fluvial sediments along the northern margin of the CIB (Hall, 2005). The main controls on fluvial architecture for the lower and middle Buntsandstein sections (Units 1 and 2) are predominantly tectonic, e.g. accommodation space and, climatic, e.g. rate and cyclicity of precipitation from the drainage basin. In contrast, the upper Buntsandstein facies (Units 3 and 4) record a progressive influence from the opening of the Tethyan seaway and advancing northward transgression prior to the highstand systems tract (HST).

## 7.2 | Implications of using sequence stratigraphy for fluvial sequences

Unconformities that are framework defining and form sequence boundaries in the marine environment are difficult to identify in the continental setting as every channel base comprises a candidate sequence boundary but can be impossible to correlate at the basin scale (e.g. Holbrook, 2001; Meadows, 2006; Shanley & McCabe, 1994). Flooding

surfaces, which have a special significance in the marine sedimentary environments, are by definition absent in the nonmarine part of the fluvial sedimentary record. This research has identified through the use of chemostratigraphy and detailed field-based correlations that the Tethyan marine transgression was rapid in the CIB with a landward stepping influence that was widespread within the basin. As a precursor to the transgression and part of the transgressive systems tract (TST), the fluvial facies and architecture underwent a transition from large, ribbon and amalgamated channel/meandering river deposits to shallow marine/estuarine facies (Figures 7, 8 and 12). The subsequent flooding resulted in the deposition of thick HST shallow marine shelfal bioclastic ramp carbonates. The additional section of fluvial sediments in the Riba de Santiuste area, identified by the chemostratigraphy, records active fluvial sedimentation in the northwest of the basin, while the south-eastern parts are already flooded (Figure 12). In addition, the absence of thick carbonates at this location, and found to the southeast, is interpreted to document the maximum landward reach of the marine transgression in this part of the basin.

Dalrymple, Kurcinka, Jablonski, Ichaso, and Mackay (2015) describes far inland reaching effects of tidal penetration in small- to medium-scale rivers for 10's to 100's Km inland. No direct tidal influence has been identified in the fluvial sediments of the upper Buntsandstein, which would be subject to potential tidal influence. This supports a rapid incursion of the Tethyan seaway and MFS with rapid shut-down of clastic fluvial sedimentation across the entire CIB. The Triassic Buntsandstein and Muschelkalk facies of latest

Anisian to early Ladinian were deposited during a time span of ~2 to 4 Ma (Figure 3; e.g. Muñoz et al., 1992; López-Gómez & Arche, 1993a, 1993b; Borrueal-Abadía et al., 2015). Assuming a transgression distance of 80 km, derived from outcrop data used in this study, a rate of transgression advance of 0.04–0.02 m/year can be estimated. Transgressive conditions lasted for 2–4 M years assuming no stillstand occurred. The advance of the Tethyan shoreline reached its most northerly extension in the CIB when most of north-eastern and central Iberia was covered by the Tethys Sea.

These rates of transgression for the Tethyan shoreline are slower than Holocene values by more than an order of magnitude. However, the rates of shoreline movement during Quaternary ice-sheet fluctuations are commonly considered to be geologically rapid, especially when compared with estimated rates of shoreline variation through geological time (e.g. Cattaneo & Steel, 2003; Evans, 1979; Leckie, 1986). The rates suggested here do not seem unreasonable. However, it is important to note the rapid cessation of all clastic input into the basin during the Tethyan transgression.

## 8 | CONCLUSIONS AND IMPLICATIONS

The Permo-Triassic Central Iberian Basin contains a >1-km-thick synrift succession deposited predominantly along the south-western faulted margin. This succession records an early alluvial fan and fluvial depositional setting, progressively evolving to shallow marine and open marine carbonate shelf with the opening of the Tethyan seaway and the advance of the marine transgression into the basin.

Sediment supply to the CIB was strongly asymmetrical early in the rift history and derived as alluvial fans from the rift shoulder. High sedimentation rates and abundant accommodation space led to the deposition of up to 200-m-thick conglomerate successions. Later during the mid-to-late synrift phases, the sediment supply became more established with the main S-SE flowing braided fluvial systems restricted along the south-eastern major rift flank. A series of high net to gross, stacked sandstones were deposited in diminishing accommodation space conditions. The latest fluvial infill records meandering or fixed channel rivers with abundant floodplain preservation. This is supported by a wetter climate favouring bank stability by vegetation growth and the lowering of the basin floor gradient due to the encroaching marine transgression.

The combination of detailed sedimentology and chemostratigraphy of the Triassic Buntsandstein sediments has allowed a high-resolution correlation of the synrift fluvial sandstones to be established. This has identified a major axially flowing fluvial system along the south-western rift margin and can be robustly correlated for ~80 km.

A chemostratigraphic correlation on the outcrop scale (Riba de Santiuste) revealed some limitations as two channel sandstones at the same palaeo-elevation can be different in age and can be derived from sediment of different mineralogical composition, thus showing a diachronous surface on the channel belt top. As a result, chemostratigraphy provides the most robust correlations at scales >1 km.

An additional section of fluvial sediments in the north-western most location (Riba de Santiuste) has been identified by the chemostratigraphy and indicates active fluvial sedimentation in the northwest of the basin, while the diachronous marine transgression has already flooded the remaining basin. The absence of thick limestone as found elsewhere in the basin at this location documents the maximum reach of the transgression into the basin. In addition, a geologically reasonable rate of advance into the basin of the marine transgression was calculated to be 0.04–0.02 m/year.

Our rift-wide study highlights the importance of robust chemostratigraphic correlations of synrift fluvial successions for understanding rift evolution, and for identifying the important rate of transition between fluvial deposition and Tethyan transgressive marine flooding of the basin. This study emphasises the important implications for correlation of nonmarine successions and especially so with encroaching marine transgressions.

## ACKNOWLEDGEMENTS

This study contains work conducted during a PhD study undertaken as part of the Natural Environment Research Council (NERC) Centre for Doctoral Training (CDT) in Oil & Gas under its Extending the Life of Mature Basins research theme. It is co-sponsored by Durham University whose support is gratefully acknowledged. Support from Chemostratigraphy Ltd, Welshpool and Redrock International allowed accurate interpretation of the chemostratigraphy correlation panels. The authors thank Sylvie Bourquin and two anonymous reviewers for their constructive feedback which greatly enhanced the quality of this article. There is no conflict of interest to declare.

## DATA AVAILABILITY STATEMENT

The data that support the findings of this study are available from the corresponding author upon reasonable request.

## ORCID

Maximilian Franzel  <https://orcid.org/0000-0002-7500-6162>

## REFERENCES

- Anders, M. H., & Schlische, R. W. (1994). Overlapping faults, intrabasin highs, and the growth of normal faults. *The Journal of Geology*, 102(2), 165–179. <https://doi.org/10.1086/629661>

- Arche, A., & López-Gómez, J. (1996). Origin of the Permian-Triassic Iberian Basin, central-eastern Spain. *Tectonophysics*, 266(1), 443–464. [https://doi.org/10.1016/S0040-1951\(96\)00202-8](https://doi.org/10.1016/S0040-1951(96)00202-8)
- Arche, A., & López-Gómez, J. (1999). Tectonic and geomorphic controls on the fluvial styles of the Eslida Formation, Middle Triassic. *Eastern Spain. Tectonophysics*, 315(1–4), 187–207. [https://doi.org/10.1016/S0040-1951\(99\)00291-7](https://doi.org/10.1016/S0040-1951(99)00291-7)
- Arche, A., & López-Gómez, J. (1999). Subsidence rates and fluvial architecture of rift-related Permian and Triassic alluvial sediments of the southeast Iberian Range, eastern Spain. *Fluvial Sedimentology VI*, 28, 288–304. <https://doi.org/10.1002/9781444304213.ch21>
- Arche, A., & López-Gómez, J. (2005). Sudden changes in fluvial style across the Permian–Triassic boundary in the eastern Iberian Ranges, Spain: Analysis of possible causes. *Palaeogeography, Palaeoclimatology, Palaeoecology*, 229(1), 104–126. <https://doi.org/10.1016/j.palaeo.2005.06.033>
- Arche, A., López-Gómez, J., Marzo, M., & Vargas, H. (2004). The siliciclastic Permian-Triassic deposits in central and northeastern Iberian Peninsula (Iberian, Ebro and Catalan basins): A proposal for correlation. *Geologica Acta*, 2(4), 305.
- Borrueal-Abadía, V., López-Gómez, J., De la Horra, R., Galán-Abellán, B., Barrenechea, J. F., Arche, A., ... Marzo, M. (2015). Climate changes during the Early-Middle Triassic transition in the E. Iberian plate and their palaeogeographic significance in the western Tethys continental domain. *Palaeogeography, Palaeoclimatology, Palaeoecology*, 440, 671–689. <https://doi.org/10.1016/j.palaeo.2015.09.043>
- Bourquin, S., Bercovici, A., López-Gómez, J., Diez, J. B., Broutin, J., Ronchi, A., ... Amour, F. (2011). The Permian-Triassic transition and the onset of Mesozoic sedimentation at the northwestern peri-Tethyan domain scale: Palaeogeographic maps and geodynamic implications. *Palaeogeography, Palaeoclimatology, Palaeoecology*, 299(1–2), 265–280. <https://doi.org/10.1016/j.palaeo.2010.11.007>
- Bourquin, S., Durand, M., Diez, J., Broutin, J., & Fluteau, F. (2007). The Permian-Triassic boundary and lower Triassic sedimentation in the Western European basins: An overview. *Journal of Iberian Geology*, 33(2), 221–236.
- Bourquin, S., Guillocheau, F., & Péron, S. (2009). Braided rivers within an arid alluvial plain (example from the Lower Triassic, western German Basin): Recognition criteria and expression of stratigraphic cycles. *Sedimentology*, 56(7), 2235–2264. <https://doi.org/10.1111/j.1365-3091.2009.01078.x>
- Bourquin, S., Péron, S., & Durand, M. (2006). Lower Triassic sequence stratigraphy of the western part of the Germanic Basin (west of Black Forest): Fluvial system evolution through time and space. *Sedimentary Geology*, 186(3), 187–211. <https://doi.org/10.1016/j.sedgeo.2005.11.018>
- Bourquin, S., Rigollet, C., & Bourges, P. (1998). High-resolution sequence stratigraphy of an alluvial fan–fan delta environment: Stratigraphic and geodynamic implications – An example from the Keuper Chaunoy Sandstones. *Paris Basin. Sedimentary Geology*, 121(3), 207–237. [https://doi.org/10.1016/S0037-0738\(98\)00081-5](https://doi.org/10.1016/S0037-0738(98)00081-5)
- Burns, B. A., Heller, P. L., Marzo, M., & Paola, C. (1997). Fluvial response in a sequence stratigraphic framework; example from the Montserrat fan delta, Spain. *Journal of Sedimentary Research*, 67(2), 311–321. <https://doi.org/10.1306/D426855E-2B26-11D7-864800102C1865D>
- Cattaneo, A., & Steel, R. J. (2003). Transgressive deposits: A review of their variability. *Earth-Science Reviews*, 62(3), 187–228. [https://doi.org/10.1016/S0012-8252\(02\)00134-4](https://doi.org/10.1016/S0012-8252(02)00134-4)
- Colombera, L., Mountney, N. P., & McCaffrey, W. D. (2015). A meta-study of relationships between fluvial channel-body stacking pattern and aggradation rate: Implications for sequence stratigraphy. *Geology*, 43(4), 283–286. <https://doi.org/10.1130/g36385.1>
- Contreras, J., Anders, M. H., & Scholz, C. H. (2000). Growth of a normal fault system: Observations from the Lake Malawi basin of the east African rift. *Journal of Structural Geology*, 22(2), 159–168. [https://doi.org/10.1016/S0191-8141\(99\)00157-1](https://doi.org/10.1016/S0191-8141(99)00157-1)
- Dalrymple, R. W., Kurcinka, C. E., Jablonski, B. V. J., Ichaso, A. A., & Mackay, D. A. (2015). Deciphering the relative importance of fluvial and tidal processes in the fluvial–marine transition. In P. J. Ashworth, J. L. Best, & D. R. Parsons (Eds.), *Developments in Sedimentology* (Vol. 68, pp. 3–45). London, UK: Elsevier.
- Dasgupta, P. (2002). Determination of paleocurrent direction from oblique sections of trough cross-stratification—A precise approach. *Journal of Sedimentary Research*, 72(1), 217–219. <https://doi.org/10.1306/050401720217>
- Davies, E. J., Ratcliffe, K. T., Montgomery, P., Pomar, L., Ellwood, B. B., & Wray, D. S. (2013). Magnetic susceptibility ( $\chi$ ) stratigraphy and chemostratigraphy applied to an isolated carbonate platform reef complex; Lluçmajor Platform, Mallorca. In K. Verwer, T. Playton, & P. Harris (Eds.), *Deposits, Architecture, and Controls of Carbonate Margin, Slope and Basinal Settings. Special Publications (105)*. Tulsa, OK: SEPM (Society for Sedimentary Geology).
- Davies, S. J., Dawers, N. H., McLeod, A. E., & Underhill, J. R. (2000). The structural and sedimentological evolution of early synrift successions: The Middle Jurassic Tarbert Formation, North Sea. *Basin Research*, 12(3–4), 343–365. <https://doi.org/10.1111/j.1365-2117.2000.00136.x>
- De la Horra, R., Galán-Abellán, A. B., López-Gómez, J., Sheldon, N. D., Barrenechea, J. F., Luque, F. J., ... Benito, M. I. (2012). Paleocological and paleoenvironmental changes during the continental Middle-Late Permian transition at the SE Iberian Ranges, Spain. *Global and Planetary Change*, 94, 46–61. <https://doi.org/10.1016/j.gloplacha.2012.06.008>
- De Vicente, G., Vegas, R., Muñoz-Martín, A., Van Wees, J. D., Casas-Sáinz, A., Sopena, A., ... Fernández-Lozano, J. (2009). Oblique strain partitioning and transpression on an inverted rift: The Castilian Branch of the Iberian Chain. *Tectonophysics*, 470(3), 224–242. <https://doi.org/10.1016/j.tecto.2008.11.003>
- DeCelles, P. G., Langford, R. P., & Schwartz, R. K. (1983). Two new methods of paleocurrent determination from trough cross-stratification. *Journal of Sedimentary Research*, 53(2), 629–642. <https://doi.org/10.1306/212F824C-2B24-11D7-8648000102C1865D>
- Diez, J. B., Bourquin, S., Broutin, J., & Ferrer, J. (2007). The Iberian Permian Triassic ‘Buntsandstein’ of the Aragonian branch of the Iberian range (Spain) in the West-European sequence stratigraphical framework: A combined palynological and sedimentological approach. *Bulletin De La Societe Geologique De France*, 178(3), 179–195. <https://doi.org/10.2113/gssgfbull.178.3.179>
- Diez, J. B., Broutin, J., Grauvogel-Stamm, L., Bourquin, S., Bercovici, A., & Ferrer, J. (2010). Anisian floras from the NE Iberian Peninsula and Balearic Islands: A synthesis. *Review of Palaeobotany and Palynology*, 162(3), 522–542. <https://doi.org/10.1016/j.revpa.2010.09.003>
- DroneRS, D. (2019). Valle de los milagros. Riba de Saelices. Retrieved from <https://youtu.be/mVBOUA3Yw-s?t=283>
- Ellwood, B. B., Tomkin, J. H., Ratcliffe, K. T., Wright, M., & Kafafy, A. M. (2008). High-resolution magnetic susceptibility and geochemistry for the Cenomanian/Turonian boundary GSSP with correlation

- to time equivalent core. *Palaeogeography, Palaeoclimatology, Palaeoecology*, 261(1), 105–126. <https://doi.org/10.1016/j.palaeo.2008.01.005>
- Evans, G. (1979). Quaternary transgressions and regressions. *Journal of the Geological Society*, 136(2), 125. <https://doi.org/10.1144/gsjgs.136.2.0125>
- Fernández, L. R. R., Olmedo, F. L., Oliveira, J. T., Medialdea, T., Terrinha, P., Matas, J., ... Nozal, F. (2015). *Mapa geológico de España y Portugal: Escala 1: 1.000.000*. Madrid, Spain: Instituto Geológico Y Minero De España (IGME).
- Flood, Y. S., & Hampson, G. J. (2017). Analysis of floodplain sedimentation, avulsion style and channelized fluvial sand-body distribution in an upper coastal plain reservoir: Middle Jurassic Ness Formation, Brent Field, UK North Sea. *Geological Society, London, Special Publications*, 444(1), 109. <https://doi.org/10.1144/SP444.3>
- Frostick, L. E., & Jones, S. J. (2002). Impact of periodicity on sediment flux in alluvial systems: Grain to basin scale. *Geological Society, London, Special Publications*, 191(1), 81–95. <https://doi.org/10.1144/GSL.SP.2002.191.01.06>
- Frostick, L. E., & Reid, I. (1989). Is structure the main control of river drainage and sedimentation in rifts? *Journal of African Earth Sciences (and the Middle East)*, 8(2), 165–182. [https://doi.org/10.1016/S0899-5362\(89\)80022-3](https://doi.org/10.1016/S0899-5362(89)80022-3)
- García-Lasanta, C., Oliva-Urcia, B., Roman-Berdiel, T., Casas, A. M., Gil-Pena, I., Sanchez-Moya, Y., ... Mattei, M. (2015). Evidence for the Permo-Triassic transtensional rifting in the Iberian Range (NE Spain) according to magnetic fabrics results. *Tectonophysics*, 651, 216–231. <https://doi.org/10.1016/j.tecto.2015.03.023>
- Gawthorpe, R. L., Fraser, A. J., & Collier, R. E. L. (1994). Sequence stratigraphy in active extensional basins: Implications for the interpretation of ancient basin-fills. *Marine and Petroleum Geology*, 11(6), 642–658. [https://doi.org/10.1016/0264-8172\(94\)90021-3](https://doi.org/10.1016/0264-8172(94)90021-3)
- Gawthorpe, R. L., & Leeder, M. R. (2000). Tectono-sedimentary evolution of active extensional basins. *Basin Research*, 12(3–4), 195–218. <https://doi.org/10.1111/j.1365-2117.2000.00121.x>
- Gupta, S., Underhill, J. R., Sharp, I. R., & Gawthorpe, R. L. (1999). Role of fault interactions in controlling synrift sediment dispersal patterns: Miocene, Abu Alaqa Group, Suez Rift, Sinai, Egypt. *Basin Research*, 11(2), 167–189. <https://doi.org/10.1046/j.1365-2117.1999.00300.x>
- Hall, P. E. (2005). *The evolution of Permo-Triassic fluvial and alluvial systems in the central Iberian basin, central Spain*. (PhD Thesis), University of Durham.
- Haq, B. U. (2018). Triassic eustatic variations reexamined. *GSA Today*, 28(12), 4–9. <https://doi.org/10.1130/GSATG381A.1>
- Hartley, A., & Evenstar, L. (2018). Fluvial architecture in actively deforming salt basins: Chinle Formation, Paradox Basin, Utah. *Basin Research*, 30(1), 148–166. <https://doi.org/10.1111/bre.12247>
- Heller, P. L., & Paola, C. (1996). Downstream changes in alluvial architecture; an exploration of controls on channel-stacking patterns. *Journal of Sedimentary Research*, 66(2), 297–306. <https://doi.org/10.1306/D4268333-2B26-11D7-8648000102C1865D>
- Hildred, G. V., Ratcliffe, K. T., Wright, A. M., Zaitlin, B. A., & Wray, D. S. (2010). Chemostratigraphic applications to low-accommodation fluvial incised-valley settings: An example from the Lower Mannville Formation of Alberta, Canada. *Journal of Sedimentary Research*, 80(11), 1032–1045. <https://doi.org/10.2110/jsr.2010.089>
- Holbrook, J. (2001). Origin, genetic interrelationships, and stratigraphy over the continuum of fluvial channel-form bounding surfaces: An illustration from middle Cretaceous strata, southeastern Colorado. *Sedimentary Geology*, 144(3), 179–222. [https://doi.org/10.1016/S0037-0738\(01\)00118-X](https://doi.org/10.1016/S0037-0738(01)00118-X)
- Jarvis, I., & Jarvis, K. E. (1992a). Inductively coupled plasma-atomic emission spectrometry in exploration geochemistry. *Journal of Geochemical Exploration*, 44(1–3), 139–200. [https://doi.org/10.1016/0375-6742\(92\)90050-I](https://doi.org/10.1016/0375-6742(92)90050-I)
- Jarvis, I., & Jarvis, K. E. (1992b). Plasma spectrometry in the earth sciences: Techniques, applications and future trends. *Chemical Geology*, 95(1–2), 1–33. [https://doi.org/10.1016/0009-2541\(92\)90041-3](https://doi.org/10.1016/0009-2541(92)90041-3)
- Jones, S. J. (2004). Tectonic controls on drainage evolution and development of terminal alluvial fans, southern Pyrenees, Spain. *Terra Nova*, 16(3), 121–127. <https://doi.org/10.1111/j.1365-3121.2004.00539.x>
- Jones, S. J., Frostick, L. E., & Astin, T. R. (2001). Braided stream and flood plain architecture: The Rio Vero Formation, Spanish Pyrenees. *Sedimentary Geology*, 139(3), 229–260. [https://doi.org/10.1016/S0037-0738\(00\)00165-2](https://doi.org/10.1016/S0037-0738(00)00165-2)
- Leckie, D. (1986). Rates, controls, and sand-body geometries of transgressive-regressive cycles: Cretaceous moosebar and gates formations, British Columbia. *AAPG Bulletin*, 70(5), 516–535. <https://doi.org/10.1306/94885944-1704-11d7-8645000102c1865d>
- Leeder, M. R., & Gawthorpe, R. L. (1987). Sedimentary models for extensional tilt-block/half-graben basins. *Geological Society, London, Special Publications*, 28(1), 139. <https://doi.org/10.1144/GSL.SP.1987.028.01.11>
- Leleu, S., Van Lanen, X. M. T., & Hartley, A. J. (2010). Controls on the architecture of a Triassic Sandy Fluvial System, Wolfville Formation, Fundy Basin, Nova Scotia, Canada: Implications for the interpretation and correlation of ancient fluvial successions. *Journal of Sedimentary Research*, 80(10), 867–883. <https://doi.org/10.2110/jsr.2010.080>
- López-Gómez, J., & Arche, A. (1993a). Sequence stratigraphic analysis and paleogeographic interpretation of the Buntsandstein and Muschelkalk facies (Permo-Triassic) in the SE Iberian Range, E Spain. *Palaeogeography, Palaeoclimatology, Palaeoecology*, 103(3–4), 179–201. [https://doi.org/10.1016/0031-0182\(93\)90142-6](https://doi.org/10.1016/0031-0182(93)90142-6)
- López-Gómez, J., & Arche, A. (1993b). Architecture of the Canizar fluvial sheet sandstones, Early Triassic, Iberian Ranges, eastern Spain. In M. Marzo, & C. Puigdefàbregas (Eds.), *Alluvial sedimentation* (pp. 363–381). London, UK: Blackwell Scientific Publications.
- López-Gómez, J., & Arche, A. (1997). The Upper Permian Boniches Conglomerates Formation: Evolution from alluvial fan to fluvial system environments and accompanying tectonic and climatic controls in the southeast Iberian Ranges, central Spain. *Sedimentary Geology*, 114(1–4), 267–294. [https://doi.org/10.1016/S0037-0738\(97\)00062-6](https://doi.org/10.1016/S0037-0738(97)00062-6)
- López-Gómez, J., Arche, A., & Pérez-López, A. (2002). Permian and triassic. In W. Gibbons, & T. Moreno (Eds.), *The geology of Spain* (pp. 185–212). London, UK: Geological Society.
- López-Gómez, J., Arche, A., Vargas, H., & Marzo, M. (2010). Fluvial architecture as a response to two-layer lithospheric subsidence during the Permian and Triassic in the Iberian Basin, eastern Spain. *Sedimentary Geology*, 223(3), 320–333. <https://doi.org/10.1016/j.sedgeo.2009.11.017>
- López-Gómez, J., Galán-Abellán, B., De La Horra, R., Barrenechea, J. F., Arche, A., Bourquin, S., ... Durand, M. (2012). Sedimentary evolution of the continental Early-Middle Triassic Cañizar Formation (Central Spain): Implications for life recovery after the Permian-Triassic crisis. *Sedimentary Geology*, 249, 26–44. <https://doi.org/10.1016/j.sedgeo.2012.01.006>

- Meadows, N. (2006). The correlation and sequence architecture of the Ormskirk sandstone formation in the Triassic Sherwood sandstone group of the East Irish Sea Basin, NW England. *Geological Journal*, 41(1), 93–122. <https://doi.org/10.1002/gj.1034>
- Miall, A. D. (1985). Architectural-element analysis: A new method of facies analysis applied to fluvial deposits. *Earth-Science Reviews*, 22(4), 261–308. [https://doi.org/10.1016/0012-8252\(85\)90001-7](https://doi.org/10.1016/0012-8252(85)90001-7)
- Miall, A. D. (1996). *The Geology of Fluvial Deposits: Sedimentary Facies, Basin Analysis, and Petroleum Geology*. Berlin, Germany: Springer.
- Muñoz, A., Ramos, A., Sánchez-Moya, Y., & Sopeña, A. (1992). Evolving fluvial architecture during a marine transgression: Upper Buntsandstein, Triassic, central Spain. *Sedimentary Geology*, 75(3–4), 257–281. [https://doi.org/10.1016/0037-0738\(92\)90096-A](https://doi.org/10.1016/0037-0738(92)90096-A)
- Newell, A. J. (2018). Evolving stratigraphy of a Middle Triassic fluvial-dominated sheet sandstone: The Otter Sandstone Formation of the Wessex Basin (UK). *Geological Journal*, 53(5), 1954–1972. <https://doi.org/10.1002/gj.3026>
- Ogg, J. G., Ogg, G., & Gradstein, F. M. (2016). *A concise geologic time scale*. London, UK: Elsevier.
- Parrish, J. T. (1993). Climate of the Supercontinent Pangea. *The Journal of Geology*, 101(2), 215–233. <https://doi.org/10.1086/648217>
- Peakall, J., Leeder, M., Best, J., & Ashworth, P. (2000). River response to lateral ground tilting: A synthesis and some implications for the modelling of alluvial architecture in extensional basins. *Basin Research*, 12(3–4), 413–424. <https://doi.org/10.1111/j.1365-2117.2000.00128.x>
- Pearce, T. J., Besly, B. M., Wray, D. S., & Wright, D. K. (1999). Chemostratigraphy: A method to improve interwell correlation in barren sequences—A case study using onshore Duckmantian/Stephanian sequences (West Midlands, UK). *Sedimentary Geology*, 124(1–4), 197–220. [https://doi.org/10.1016/S0037-0738\(98\)00128-6](https://doi.org/10.1016/S0037-0738(98)00128-6)
- Pearce, T. J., Martin, J. H., Cooper, D., & Wray, D. S. (2010). Chemostratigraphy of upper carboniferous (Pennsylvanian) sequences from the Southern North sea (United Kingdom). In K. Ratcliffe, & B. A. Zaitlin (Eds.), *Application of modern stratigraphic techniques: Theory and case histories*: SEPM Special Publication (Vol. 94, pp. 109–127). Tulsa, OK: SEPM.
- Pearce, T. J., Wray, D. S., Ratcliffe, K. T., Wright, D. K., & Moscariello, A. (2005). Chemostratigraphy of the Upper Carboniferous Schooner Formation, southern North Sea. *Carboniferous Hydrocarbon Geology: The Southern North Sea and Surrounding Onshore Areas: Yorkshire Geological Society, Occasional Publications Series, 7*, 147–164.
- Pe-Piper, G., Triantafyllidis, S., & Piper, D. J. (2008). Geochemical identification of clastic sediment provenance from known sources of similar geology: The Cretaceous Scotian Basin. *Canada. Journal of Sedimentary Research*, 78(9), 595–607. <https://doi.org/10.2110/jsr.2008.067>
- Pisel, J. R., Pyles, D. R., & Kirschbaum, M. A. (2018). The influence of lateral topographic confinement on fluvial channel-belt clustering, compensation and connectivity – Lower Wasatch Formation and Dakota Sandstone, Utah, USA. *Sedimentology*, 65(2), 597–619. <https://doi.org/10.1111/sed.12395>
- Posamentier, H., Jervey, M., & Vail, P. (1988). Eustatic controls on clastic deposition I—Conceptual framework. In C. Wilgus, B. Hastings, C. C. Kendall, H. Posamentier, C. Ross, & J. Van Wagoner (Eds.), *Sea-level changes: An integrated approach* (Vol. 42, pp. 109–124). Tulsa, OK: SEPM.
- Posamentier, H., & Vail, P. (1988). Eustatic controls on clastic deposition II—Sequence and systems tract models. In C. Wilgus, B. Hastings, C. C. Kendall, H. Posamentier, C. Ross, & J. Van Wagoner (Eds.), *Sea-level changes: An integrated approach* (Vol. 42, pp. 125–154). Tulsa, OK: SEPM.
- Preto, N., Kustatscher, E., & Wignall, P. B. (2010). Triassic climates — State of the art and perspectives. *Palaeogeography, Palaeoclimatology, Palaeoecology*, 290(1), 1–10. <https://doi.org/10.1016/j.palaeo.2010.03.015>
- Prosser, S. (1993). Rift-related linked depositional systems and their seismic expression. *Geological Society, London, Special Publications*, 71(1), 35. <https://doi.org/10.1144/GSL.SP.1993.071.01.03>
- Ramos, A., Sopena, A., & Perez-Arlucea, M. (1986). Evolution of Buntsandstein fluvial sedimentation in the Northwest Iberian Ranges (central Spain). *Journal of Sedimentary Petrology*, 56(6), 862–875. <https://doi.org/10.1306/212F8A6C-2B24-11D7-8648000102C1865D>
- Ratcliffe, K., Wilson, A., Payenberg, T., Rittersbacher, A., Hildred, G. V., & Flint, S. S. (2015). Ground truthing chemostratigraphic correlations in fluvial systems. *AAPG Bulletin*, 99(1), 155–180. <https://doi.org/10.1306/06051413120>
- Ratcliffe, K., Wright, M., Montgomery, P., Palfrey, A., Vonk, A., Vermeulen, J., & Barrett, M. (2010). Application of chemostratigraphy to the Mungaroo Formation, the Gorgon field, offshore north-west Australia. *The APPEA Journal*, 50(1), 371–388. <https://doi.org/10.1071/AJ09022>
- Salas, R., & Casas, A. (1993). Mesozoic extensional tectonics, stratigraphy and crustal evolution during the Alpine cycle of the eastern Iberian basin. *Tectonophysics*, 228(1–2), 33–55. [https://doi.org/10.1016/0040-1951\(93\)90213-4](https://doi.org/10.1016/0040-1951(93)90213-4)
- Salas, R., Guimerà, J., Mas, R., Martín-Closas, C., Meléndez, A., & Alonso, A. (2001). Evolution of the Mesozoic central Iberian Rift System and its Cainozoic inversion (Iberian chain). *Peri-Tethys Memoir*, 6, 145–185.
- Sano, J. L., Ratcliffe, K. T., & Spain, D. R. (2013). Chemostratigraphy of the Haynesville Shale. In U. Hammes & J. Gale (Eds.), *Geology of the Haynesville Gas Shale in East Texas and West Louisiana, USA: AAPG Memoir 105* (pp. 137–154). Tulsa, OK: The American Association of Petroleum Geologists.
- Schlische, R. W. (1991). Half-graben basin filling models: New constraints on continental extensional basin development. *Basin Research*, 3(3), 123–141. <https://doi.org/10.1111/j.1365-2117.1991.tb00123.x>
- Shanley, K. W., & McCabe, P. J. (1991). Predicting facies architecture through sequence stratigraphy—An example from the Kaiparowits Plateau, Utah. *Geology*, 19(7), 742–745. [https://doi.org/10.1130/0091-7613\(1991\)019<0742:PFATSS>2.3.CO;2](https://doi.org/10.1130/0091-7613(1991)019<0742:PFATSS>2.3.CO;2)
- Shanley, K. W., & McCabe, P. J. (1994). Perspectives on the sequence stratigraphy of continental strata. *AAPG Bulletin*, 78(4), 544–568. <https://doi.org/10.1306/bdff9258-1718-11d7-8645000102c1865d>
- Sopeña, A., López, J., Arche, A., Pérez-Arlucea, M., Ramos, A., Virgili, C., & Hernandez, S. (1988). Permian and Triassic rift basins of the Iberian Peninsula. In *Developments in Geotectonics* (Vol. 22, pp. 757–786). London, UK: Elsevier.
- Svendsen, J., Friis, H., Stollhofen, H., & Hartley, N. (2007). Facies discrimination in a mixed fluvio-eolian setting using elemental whole-rock geochemistry—Applications for reservoir characterization. *Journal of Sedimentary Research*, 77(1), 23–33. <https://doi.org/10.2110/jsr.2007.008>

- Van Wees, J. D., Arche, A., Beijdorff, C. G., López-Gómez, J., & Cloetingh, S. A. P. L. (1998). Temporal and spatial variations in tectonic subsidence in the Iberian Basin (eastern Spain): Inferences from automated forward modelling of high-resolution stratigraphy (Permian–Mesozoic). *Tectonophysics*, *300*(1), 285–310. [https://doi.org/10.1016/S0040-1951\(98\)00244-3](https://doi.org/10.1016/S0040-1951(98)00244-3)
- Wright, A. M., Ratcliffe, K. T., Zaitlin, B. A., & Wray, D. S. (2010). The application of chemostratigraphic techniques to distinguish compound incised valleys in low-accommodation incised-valley systems in a foreland-basin setting: An example from the Lower Cretaceous Mannville Group and Basal Colorado Sandstone (Colorado Group), Western Canadian Sedimentary Basin. In K. Ratcliffe, & B. A. Zaitlin (Eds.), *Application of modern stratigraphic techniques: Theory and case histories* (Vol. 94, pp. 93–107). Tulsa, OK: SEPM.
- Young, M. J., Gawthorpe, R. L., & Sharp, I. R. (2002). Architecture and evolution of syn-rift clastic depositional systems towards the tip of a major fault segment, Suez Rift. *Egypt. Basin Research*, *14*(1), 1–23. <https://doi.org/10.1046/j.1365-2117.2002.00162.x>

**How to cite this article:** Franzel M, Jones SJ, Meadows N, Allen MB, McCaffrey K, Morgan T. Basin-scale fluvial correlation and response to the Tethyan marine transgression: An example from the Triassic of central Spain. *Basin Res.* 2021;33:1–25. <https://doi.org/10.1111/bre.12451>